Determining the speed of sound in curved bones

by

Mark Maarten Vermeulen

to obtain the degree of Bachelor of Science
at the Delft University of Technology,
to be defended publicly on Thursday the 24th of February, 2022.

Student number:	4867327	
Project duration:	5th February 2021 – 24th February 2022	
Supervision:	ir. M. Mozaffarzadeh,	TU Delft
	Prof. dr. ir. C. Vuik,	TU Delft
	Prof. dr. ir. N. De Jong,	TU Delft
Thesis committee:	Prof. dr. ir. C. Vuik,	TU Delft, supervisor
	Dr. ir. M. D. Verweij,	TU Delft
	Dr. J. L. A. Dubbeldam,	TU Delft
	Dr. ir. D. J. Verschuur,	TU Delft

An electronic version of this thesis is available at http://repository.tudelft.nl/.

TU Delft

Contents

Layman's summary **1**

Abstract **3**

1 Introduction **5**
1.1 Theoretical background 6
1.1.1 The head wave 6
1.1.2 The bidirectional method 6
1.1.3 The semblance method 7
1.2 Prior research 8
1.2.1 Technical developments 8
1.2.2 Clinical applications 9
1.2.3 Conclusion 10

2 Experimental method **11**
2.1 Derivation of the trajectories 11
2.1.1 Flat bone 11
2.1.2 Semicircular bone 13
2.1.3 Numerical method for arbitrary geometry 14
2.2 Computer simulation of the measurements 14
2.3 Data analysis of the simulation results 16

3 Results **19**
3.1 Comparison with bidirectional method 19
3.1.1 Flat interface 19
3.1.2 Tilted interface 20
3.1.3 Semicircular interface 22

4 Discussion **29**

5 Conclusion **33**

Appendix A: Derivation of the critical angle for a flat bone **33**

Appendix B: Convergence test **36**

Layman’s summary

The goal of this project is to find a way to determine the speed of sound in curved bones. This speed of sound can then be used to make higher quality ultrasound images of the brain, and to diagnose a disease called osteoporosis. There is already a technique to find the speed of sound in flat bones, which is called bidirectional axial transmission. This technique relies on making a sound wave propagate along the surface of the bone. Bones with a curved surface thus respond differently to these kinds of measurements. In this project, we calculate what this difference is, and use this information to create a new technique that accounts for this difference. For semicircular bones it can be calculated directly. For bones with any other shape it can be calculated by a computer. We also use a computer to simulate some measurements on flat, tilted and curved bones. For curved bones, the new technique works much better than the old technique, but the old technique works somewhat better for the flat and tilted bones.

Abstract

Current research on osteoporosis detection and transcranial imaging suggests that it is necessary to find a method to calculate the speed of sound in curved bones. A popular method to find the speed of sound in bones is by the bidirectional axial transmission technique. Currently, this method assumes that the arrival time of the head wave depends linearly on the source-receiver distance. For curved bones this assumption is not valid. The arrival time of the head wave as a function of the source-receiver distance follows a curved trajectory. In this report, we attempt to find an extension to the current method that also works for curved bones, and evaluate how accurate the results of this extended method are.

This extension is based on the semblance method, that quantifies how well a certain trajectory agrees with the received data. In the first part of our project, theoretical trajectories are calculated for flat and semicircular bones. Furthermore, a numerical method is discussed to find these trajectories for arbitrary geometries. Comparing the trajectories corresponding to different velocities using the semblance methods allows for the determination of the speed of sound.

The accuracy of this extended method is evaluated by computer simulations. In these simulations, a Philips P4-1 Cardiac Sector Probe consisting of 96 elements was used to perform measurements on three different geometries. These geometries consisted of three different single interfaces between water (simulating soft tissue) and bone. The first interface consists of a straight interface between a 2 mm thick layer of water and a 5 mm thick layer of bone (that continues until the bottom edge of the simulation). The second simulation is the same, but the interface is rotated 2 degrees around its midpoint. In the third and fourth simulation, the interface is a semicircle with a 50 mm and 40 mm radius, respectively. The speed of sound in the bone was taken to be 3 mm/μs. The received data was interpolated by a cubic interpolation with a refinement of 4. Both the bidirectional and the extended, trajectory-based method were applied on the raw and interpolated data.

For the flat interface, the bidirectional method performed slightly better than the trajectory-based method (0.13% and 0.30% error, respectively). The same is true for the tilted interface (0.16% and 0.23% error). Interpolation did not affect the results here. For the 50 mm semicircular interface, the trajectory-based method performed much better than the bidirectional method: it had a 0.10% error compared to a 2% one. This was also true when the interpolation was applied: then the errors were 0.3% and 1.97%. Similar improvements were seen for the 40 mm radius semicircle. The higher error of the trajectory-based method for the flat and tilted interfaces can be explained by small errors in the additional assumptions that this method makes.

One drawback of the trajectory-based method is that there can be problems interpreting the results. This can be seen in the semblance plots, which plot the semblance coefficient (how well the trajectory fits the data) against the test velocity. For the bidirectional method, these plots clearly have a single biggest peak. For the trajectory-based methods the plot contains multiple large peaks. Furthermore, for the semicircular bone this plot contains a flat peak, which can cause multiple test velocities to have approximately the same semblance. This is a problem, since it means that small changes to the experimental setup can cause big changes in the calculated velocity. Indeed, this can be seen for the trajectory-based method on the 40 mm radius semicircular bone, which has a 1.6% error without interpolation (0.43% with interpolation). Further research could examine solutions to this problem, such as increasing the window size of the semblance method, taking the average velocity over flat peaks, or using an alternative to the semblance method. Finally, we conclude that the trajectory-based method represents an improvement over the bidirectional method when examining curved bones.

1 Introduction

Osteoporosis is a disease that causes affected bones to become porous and brittle. There are many methods to diagnose osteoporosis: the most common ones are called dual-energy X-ray attenuation (DXA) and peripheral quantitative computed tomography (pQCT). While these methods are effective, they are expensive and it is difficult to move the equipment around. This has motivated the search for a method to diagnose osteoporosis using ultrasound waves [1]. One of these methods is called head wave axial transmission. The axial transmission method, first introduced in a paper by Lowet and Van der Perre, uses two probes held perpendicularly to the bone that is being investigated [2]. An example of such an axial transmission setup is shown in figure 1.1. The results from an axial transmission measurement can be used to determine the speed of sound in the bone material, but currently this is only possible for bones with a flat near surface (on the side of the transmitter and receiver).
Current research in transcranial ultrasound imaging [3]–[5] has shown the need for a technique to accurately measure the speed of sound in curved bones. An unrelated study by Daugschies et al. [6] proposes a technique to measure the fracture risk of certain bones. For this technique, it is necessary to measure the speed of sound along a tangential path, which is often curved. These two developments provide a motivation for extending the head wave axial transmission method to curved bones.

In this research project, we will try to create this extension, called the trajectory-based method in this report. Our extension will give the correct result for any bone geometry, as long as this geometry is known beforehand. This geometry can be found using conventional beamforming techniques (such as the delay-and-sum technique) [5], [7]. Our main aim is to find out how the curvature of a bone-water interface influences the head wave axial transmission technique, and whether our extension compensates for this influence. To this end, the wave path of the first arriving signal (FAS) in the axial transmission technique is derived. This is first done analytically for a straight bone-water interface, and later numerically for a curved bone. Secondly, axial transmission measurements are simulated for bones with straight, tilted and curved interfaces. These simulations are done using the SimSonic2D

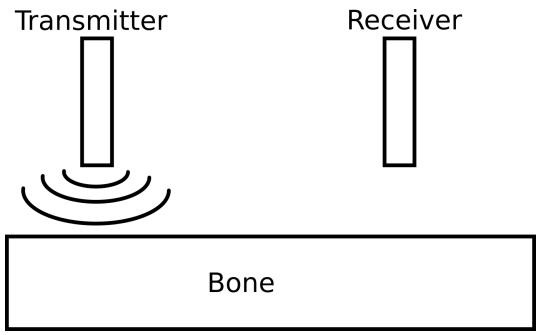

Figure 1.1: An example of the axial transmission setup used in Lowet et al.

software package (www.simsonic.fr) [8]. The results of these simulations are analysed to compare the bidirectional axial transmission method to the proposed extended method.

In chapter 2 of this report, the experimental method is discussed. Chapter 3 contains the results and in chapter 4 the results will be discussed. Finally, chapter 5 contains a conclusion.

1.1. Theoretical background

1.1.1. The head wave

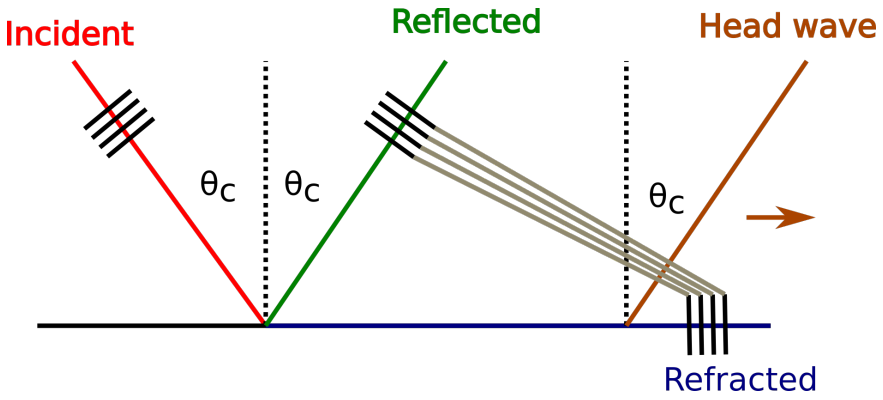

Figure 1.2: Diagram showing how the head wave is excited on a flat interface. Here θ_c is the critical angle. The black and grey lines represent the amplitude of the wavefronts. The red line corresponds to the incident, the green line to the reflected, the blue line to the refracted and the brown line to the head wave.

The head wave is a physical phenomenon that was first discovered in 1910 from earthquake records [9]. Today it is primarily used in geology, for example to investigate rock layers. The head wave can occur at the interface between two media with different speeds of sound. From these speeds of sound c_1 and c_2, we can calculate the critical angle by: $\theta_c = \arcsin(c_1/c_2)$ [9]. If a wave approaches the interface at this critical angle, it will be reflected and refracted. The reflected wave will exit the medium at the same angle θ_c, but the refracted wave will continue along the surface. This phenomenon is called total internal reflection. An example is shown in figure 1.2. It can be seen that the refracted wave travels along the interface. This is however not consistent with the boundary conditions, which require the pressure and normal displacement to be equal on both sides of the interface [9]. To solve this, there must be a wavefront linking the refracted and reflected wave, shown in grey in figure 1.2. A careful examination of this wavefront reveals that it can be represented as a ray, which we call the head wave. This ray exits the interface at the critical angle θ_c. The point where this happens moves along the interface. This is because the head wave must keep up with the refracted wave, which propagates along the surface.
Because of this sweeping action, a receiver that is positioned above the interface only detects the head wave once. This is because the wave is only detected when the head wave ray intersects the receiver. An example of this is given by the red line in figure 2.1. This path shows that the wave enters the bone at the critical angle, then propagates along the surface, and finally exits the bone at the critical angle. Lowet and Van der Perre have have conducted experiments on rectangular bones that confirm these paths [2]. However, for very thin bones (if the wavelength inside the bone layer is larger than the thickness of the bone layer) the ray approximations done above cannot be justified. Instead, the signal will propagate trough the bone as a lamb wave mode [10]. The same experiments from Lowet and Van der Perre seem to suggest that the head wave follows the quickest path from transmitter to receiver. As we will see later in this report, this is not the case for curved bones.

1.1.2. The bidirectional method

Early in the development of the head wave axial transmission technique for bones, a problem was identified. The travel time of the head wave would be different if the transmitter and receiver were skewed with respect to the interface. This, in turn, caused problems determining the velocity of the head wave. Since the end goal was to apply the technique to bones, that are covered by a layer of skin that is not

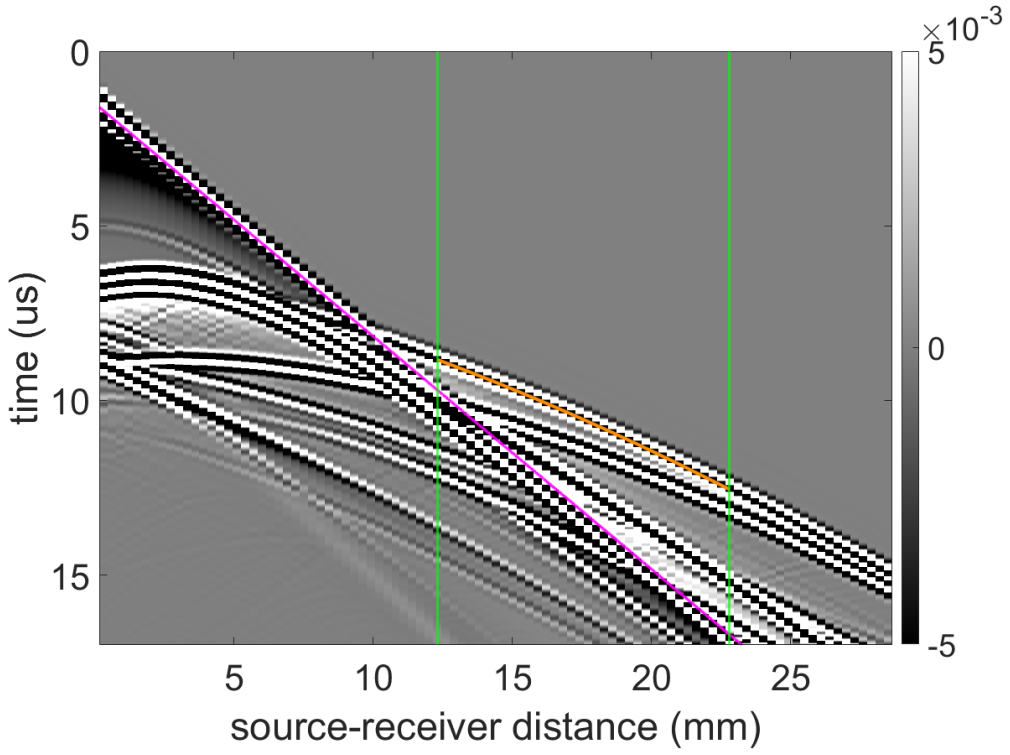

Figure 1.3: Example x-t diagram with an applied mask. The brightness at each point of the graph represents the vertical speed of the medium. The pink line corresponds to the direct wave. The green lines represent the outer limits of the mask, while the orange line corresponds to the trajectory found by the semblance method.

exactly straight, this was a major obstacle.
To solve this, Bossy et al. proposed a new technique [11]. This consisted of taking two separate measurements: one for the wave propagating to the right (forward transmission), and one for propagation to the left (reverse transmission). If v_f and v_r are the velocities obtained from this forward and reverse propagation, and α is the angle of the interface with respect to the probe, then the corrected velocity is given by[1] (found in, among others, [12])

$$v = \frac{2v_f v_r \cos(\alpha)}{v_f + v_r} \tag{1.1}$$

For small angles α this reduces to twice the harmonic mean of v_f and v_r, which is no longer dependent on α. While this method is very effective for inclined surfaces, it still requires the bones to be rectangular in shape. If the bones are curved or irregularly shaped, this correction quickly becomes inaccurate.

1.1.3. The semblance method

The semblance method is a way of determining the speed of a certain wavefront from an x-t diagram. This x-t diagram contains the intensity of the signal at time a t at a receiver with source-receiver distance x. An example can be seen in figure 1.3.

An x-t diagram often contains more than one wavefront, so first a region is chosen where the signal of interest is present and clearly distinct from the other wavefronts. This can be done by manually looking at the diagram, or by deriving a condition mathematically. Then the x-t diagram is *masked*: the intensity at all points outside the region of interest is set to zero. The exact shape of the mask varies depending on which wavefronts must be extracted. In figure 1.3 the mask is indicated by the two green lines. The mask in this figure is the region $12.3 < x < 22.8$ mm. Indeed, outside this region

[1] In Bossy et al. [11] there is an equivalent formula that is off by a factor 2. We believe this to be a misprint, as e.g. in Renaud et al. [12] this factor is present.

the wavefront of interest (indicated by the orange line) start interfering with the direct wave (indicated by the pink line) or with a reflected wave (for $x > 20$ mm).

Next, we must determine the velocity of the wavefront. It is often possible to assume the velocity is in a certain range $[V_-, V_+]$. A number of test velocities V_{est} are then taken from this range. For each test velocity a trajectory $t(x)$ is calculated. For a rectangular bone, we expect the head wave to follow a straight line in the (x,t)-plane. The trajectory can then be given by:

$$t(x) = t_{int} + (x - x_{int})/V_{est}$$

Where t_{int} and x_{int} are any coordinates on the path of the signal of interest. In the case of rectangular bones, these coordinates are found by looking at the data of the first receiver (corresponding to the lowest x-value after the mask has been applied). The first signal in time in this data corresponds to the first arriving signal, and in this situation that will be the head wave. For our extension to curved bones, a different trajectory is used. More information on this extension is given in the experimental methods section.

To make the following calculations easier, the trajectory is transformed to give the time index j as a function of the receiver index i. It then becomes:

$$j(i) = \text{round}\left(\frac{t_{int} + (i \cdot dr - x_{int})/V_{est}}{dt}\right) \tag{1.2}$$

Where dr is the pitch between the receivers and dt the time step of the recorded signals. The semblance coefficient S is then calculated along this trajectory using:

$$S = \frac{\sum_{j=-N/2}^{+N/2}\left(\sum_{i=1}^{N_r} f_{i,j(i)}\right)^2}{N_r \sum_{j=-N/2}^{+N/2}\sum_{i=1}^{N_r} f_{i,j(i)}^2} \tag{1.3}$$

Where N_r is the total number of receivers and $f_{i,j}$ is the amplitude of the signal from receiver number i at time index j. N is the window size in the time domain. For the case $N = 1$, the sum is only over the trajectory. If $N > 1$, then the sum is over a band following the trajectory with width N in the time axis. In this project, only $N = 1$ is used. The motivation of this semblance coefficient is that it gives the ratio of two energies: The numerator corresponds to the energy of the sum of all the amplitudes along the trajectory, while the denominator corresponds to the energy of all the amplitudes individually. Therefore, the trajectory with the highest semblance coefficient is the best fit for the data. From this it can be concluded that the V_{est} that corresponds to the highest semblance coefficient is the actual velocity of the wavefront.

1.2. Prior research

1.2.1. Technical developments

The behaviour of acoustic waves has long been a topic of interest in geology. In fact, the head wave was first discovered by looking at earthquake records [9]. It is in this context that I. Lerche first investigated the effect of the head wave reflecting off of a curved surface [13]. In this way, he hoped to be able to look at the structure of the subsurface rock layers. He concluded that under certain circumstances curved surfaces increase the amplitude of the head wave. Furthermore, curved surfaces cause the amplitude of the head wave to be frequency-dependent.

The first proposal to use the head wave to examine bones was made by Lowet et al. in 1996 [2]. They used an axial transmission setup that is very similar to the one in this paper, with a transmitter and receiver placed some distance above and perpendicular to the bone (modelled as a flat bar). They proposed a wave path entering at the critical angle, propagating along the surface of the bone, and then exiting at the critical angle towards the receiver. Though they did not explicitly state this, they were dealing with the head wave. Using linear regression, the speed of sound in the bone was calculated from the arrival time of this head wave. In this way, the influence of a flat layer of soft tissue above

the bone is compensated away. The speed of sound, they proposed, contained information about the composition and thus health of the bone. Furthermore, they showed that it is in theory possible to detect fractures from the axial transmission data.

A paper by Camus et al. in 2000 showed that Lowet et al. indeed measured the head wave [9]. Furthermore, since this was the case, they showed that a simpler and more physically appropriate derivation of the wave path was possible. Later, in 2002, Bossy et al., using a computer simulation, found that the first arriving signals in these axial transmission measurements is not always the head wave [10]. For a flat plate, the thickness of the plate determines which wave arrives first. If this thickness is greater than the wavelength, the head wave arrives first. If it is smaller than 0.25λ, the S_0 lamb wave mode arrives first. In between there is a complex situation that causes the first arriving signal to depend on many factors.

In 2004, more attention was given to the fact that bones are not flat plates. First, Bossy et al. concluded that hollow tubes can be modelled accurately as flat planes [8]. Furthermore, they found that curvature perpendicular to the axis of propagation has no effect on the measured speed of sound. Later that same year they published a paper introducing the bidirectional axial transmission method [11]. This method involves taking two axial transmission measurements in opposite directions. By doing this, it is possible to compensate for the effect of the probe being angled with respect to the bone. While this thus negates the effect of an angled layer of soft tissue above the bone, it does not work when this layer is curved or irregularly shaped. More information on the bidirectional method is given in the theoretical background section.

This last issue was largely solved in 2008 when Pham et al. did a simulation study [14]. They used a CT scan of actual bone samples to generate the geometry for the simulation. Their result was that the bone geometry can be accurately modelled as a tilted plate, at least in the axial direction.

In 2017, Gräsel et al. attempted to measure bone anisotropy [15]. To do this, they created a special probe that can measure the speed of sound along multiple angles. Since the tangential direction of the bone is often curved, they also briefly discussed the effects of curvature. In their situation, they could account for these effects by a simple linear regression. However, this is not possible for strong or nonuniform curvatures. Furthermore, they did not fully explain what effects this curvature has on the head wave.

1.2.2. Clinical applications

In parallel with the technical development of the method, the suitability for clinical purposes was also evaluated. In 2002, Nicholson et al. attempted to diagnose osteoporosis using axial transmission [16]. They showed that for a plate thinner than 0.5λ, the axial transmission method approached the propagation speed of the S_0 lamb wave mode, instead of the head wave. Furthermore, they found that this lamb wave was better suited for diagnosing osteoporosis.

P. Moilanen also looked at the diagnosis of osteoporosis. In his 2008 literature review, he found that ultrasonic axial transmission has advantages over the competing pQCT and DXA techniques [1]. Among others, it has no ionising radiation, it can be used to determine elastic properties of bone and it is cheaper and more portable.

In 2009 Talmant et al. looked at using the axial transmission method to estimate bone fracture risk, instead of diagnosing osteoporosis [17]. They found that the axial transmission method outperformed the then conventional DXA method. Furthermore, they proposed a measurement technique based on rotating the probe, that eliminated rotational positioning errors.

Daugschies et al., on the other hand, looked at directly measuring the anisotropy of bone in 2014 [6].

Their method requires also measuring the speed of sound in the tangential directions, which is often strongly curved in real-life measurements. This also provides a motivation to look at the behaviour of the head wave in curved surfaces.

1.2.3. Conclusion

While Gräsel et al. [15] briefly noted the effect of curvature, they did not fully explain the effects of this curvature. Furthermore, they did not measure the effect in bones with strong curvature, such as very long bones or the skull. We thus conclude that there is still a need for research focussing extensively on the effect of a curved surface on the head wave method.

2

Experimental method

2.1. Derivation of the trajectories

An important part of the proposed method are trajectories. These are functions that give the arrival time t of the head wave as a function of the source-receiver distance r. As explained in the introduction, the semblance method quantifies how well a certain trajectory agrees with the received data. The trajectory of the head wave depends on the speed of sound in the bone. Therefore, by testing trajectories corresponding to different velocities, the true speed of sound in the bone can be found.

In this section, methods to find these trajectories will be discussed. For simple geometries, these trajectories can be found analytically. For arbitrary geometries, on the other hand, a numerical method will be discussed.

2.1.1. Flat bone

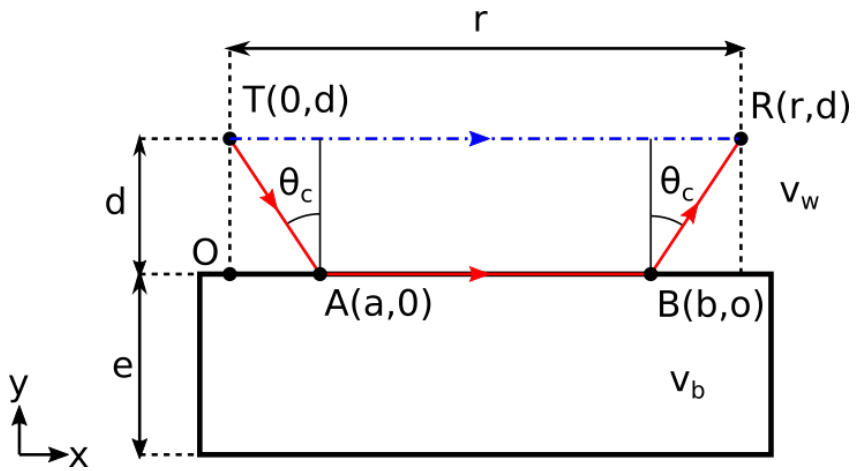

Figure 2.1: A drawing of the experimental setup. The rectangle with the solid borders is the bone sample. T is the transmitter and R is the receiver. O is the origin of the coordinate system, and A and B are the points where the head wave enters and exits the bone. The distance between the transmitter and the receiver is r, the vertical distance between the transmitter and the bone surface is d, and the thickness of the bone is e. θ_c is the critical angle that is described later in this report. The blue dot-dashed line corresponds to the path of the direct wave, while the solid red line corresponds to the head wave. The probe used in the actual measurements consists of 1 transmitter and 95 receivers in a fixed arrangement. This was modelled mathematically by varying the value of r.

In this section the trajectory corresponding to head wave is derived for a flat bone. This has also been done in less detail in Lowet et al. and Camus et al. [2], [9], but it is repeated here to motivate the extension to curved bones and arbitrary geometries.

The situation is sketched in figure 2.1. It consists of a rectangular piece of bone where the lateral speed

of sound is v_b surrounded by soft tissue with speed of sound v_w. This surrounding tissue is modelled as water, which has similar acoustic properties. An ultrasonic transmitter is placed at point T$(0, d)$ and a receiver at point R(r, d). Since the speed of sound is homogeneous in water, the direct wave is a straight line from T to R. It is shown as the blue dot-dashed line in figure 2.1. The time it takes for the direct wave to arrive is given by:

$$t_{\text{direct}} = \frac{r}{v_w} \tag{2.1}$$

The head wave is shown as the solid red line in figure 2.1.

Since the speed of sound is homogeneous in water and in bone, waves will travel in a straight line inside both media. Therefore, the only degrees of freedom in the system are the points where the head wave enters the bone (point A) and where it exits the bone (point B). Since the bone surface is straight, the coordinates of A are $(a, 0)$ and those of B are $(b, 0)$.

Then we can give the arrival time of the head wave by:

$$t_{\text{head}} = \frac{\sqrt{a^2 + d^2}}{v_w} + \frac{b - a}{v_b} + \frac{\sqrt{(r - b)^2 + d^2}}{v_w} \tag{2.2}$$

Where the first term corresponds to the line segment TA, the second to AB and the third to BR.

It remains to find the values of a and b. An important property of the head wave is that it always enters and exits media at the same angle to the normal. This angle is called the critical angle, and it is given by:

$$\sin(\theta_c) = \frac{v_w}{v_b} \tag{2.3}$$

A derivation of this formula is given in appendix A. Since the angle between T, A and the vertical is θ_c, we see $a = d\tan(\theta_c)$. Similarly, the angle between R, B and the vertical gives $r - b = d\tan(\theta_c)$. Now the critical angle from equation 2.3 gives:

$$\tan(\theta_c) = \tan\left(\arcsin\left(\frac{v_w}{v_b}\right)\right) = \frac{\frac{v_w}{v_b}}{\sqrt{1 - \left(\frac{v_w}{v_b}\right)^2}} = \frac{1}{\sqrt{\left(\frac{v_b}{v_w}\right)^2 - 1}} \tag{2.4}$$

The second to last equality follows from $0 < v_w < v_b$, and that $\tan(\arcsin(x)) = x/\sqrt{1 - x^2}$ for $|x| < 1$. This identity finally gives the value of a and b:

$$a = r - b = d\tan(\theta_c) = d\left(\sqrt{\left(\frac{v_b}{v_w}\right)^2 - 1}\right)^{-1} \tag{2.5}$$

Substituting this into equation 2.2 and simplifying gives the final result for the trajectory:

$$t_{\text{head}} = \frac{r}{v_b} + \frac{2d}{v_w}\sqrt{1 - \left(\frac{v_w}{v_b}\right)^2} \tag{2.6}$$

Which agrees with equation 6 from [9], keeping in mind that in our model the transmitter and receiver have the same vertical position.

To set up the data analysis correctly, it can sometimes be useful to know for which source-receiver distances r the head wave arrives before the direct wave. This condition can now be found using equations 2.1 and 2.6:

$$t_{\text{head}} < t_{\text{direct}} \Rightarrow r > \frac{2dv_b}{v_b - v_w}\sqrt{1 - \left(\frac{v_w}{v_b}\right)^2} \tag{2.7}$$

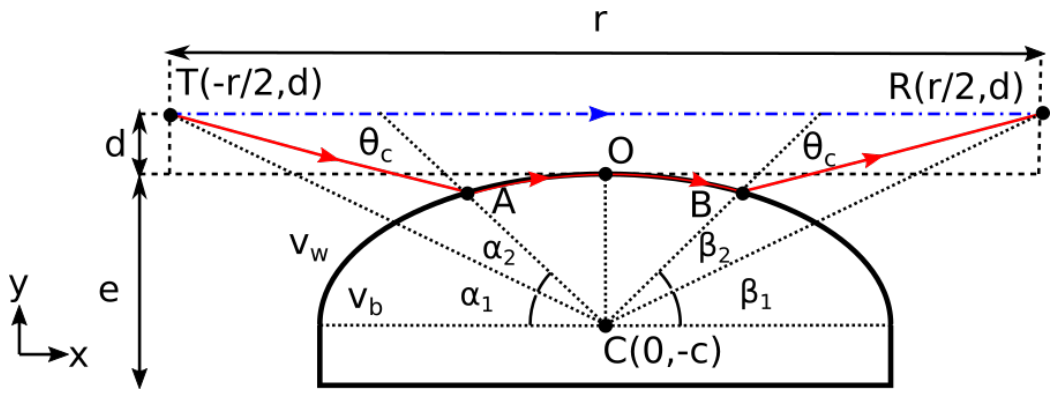

Figure 2.2: A drawing of the experimental setup for curved bones. The semicircle with the solid borders is the bone sample. T is the transmitter, R is the receiver and C is the center of the semicircle. O is the origin of the coordinate system, and A and B are the points where the head wave enters and exits the bone. The blue dot-dashed line corresponds to the path of the direct wave, while the solid red line corresponds to the head wave. Note that the drawing shows an ellipse, but that the calculations were done on a real semicircle.

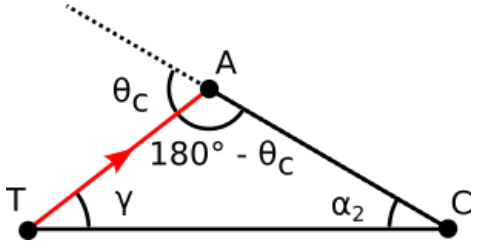

Figure 2.3: This is a schematic representation of the triangle between points A, T and C in figure 2.2.

2.1.2. Semicircular bone

Since the aim of this project is to find the speed of sound in curved bones, we must extend the results of the last section to semicircular bones. Lowet and Van der Perre [2] derive their hypotheses for the head wave path from a least time criterion: the head wave travels along the path that minimises the propagation time from transmitter to receiver. Their investigation of bars with defects (figures 9b and 9c of their article) seems to imply that it is possible for the head wave to propagate into the bone, if this results in a lower total propagation time.

Later research [9] has utilised a different approach to finding the head wave path. In this article, Camus et al. argue that the head wave arises as a result of the boundary conditions at the interface between two media. From this perspective, it would not be possible for the head wave to travel into the bone material, as it would then stop being able to satisfy the boundary condition. For this report we have chosen to apply the more current interpretation of the head wave in terms of boundary conditions. As a result of this, the head wave travels along the surface of the bone, even when that is not absolutely the quickest path.

Like in the case for a flat bone, we assume that the head wave enters the bone at the critical angle. Since the bone is curved, this critical angle must be taken with respect to the normal at the surface. This normal is now no longer always the vertical. The geometry of the bone, and of the head wave path under these assumptions, is shown in figure 2.2.

The bone geometry is a semicircle with radius c and center point C. To make the calculations easier, the origin of the coordinate system is moved to the middle of the bone (directly above the center point C). Furthermore, point A and B, where the wave enters and exits the bone, are no longer characterised by their x-coordinate. Instead, they are characterised by the angle α and β they make to the horizontal. The position of A is thus given by $(-c\cos(\alpha), -c + c\sin(\alpha)$ and the position of B is given by $(c\cos(\beta), -c + c\sin(\beta))$. In the figure $\alpha = \alpha_1 + \alpha_2$ and $\beta = \beta_1 + \beta_2$.

In our situation α_1 and β_1 are known, as they are the slope of the lines CT and CR, and the positions C, T, and R are known. Thus the wave path is known if α_2 and β_2 can be calculated. These can be

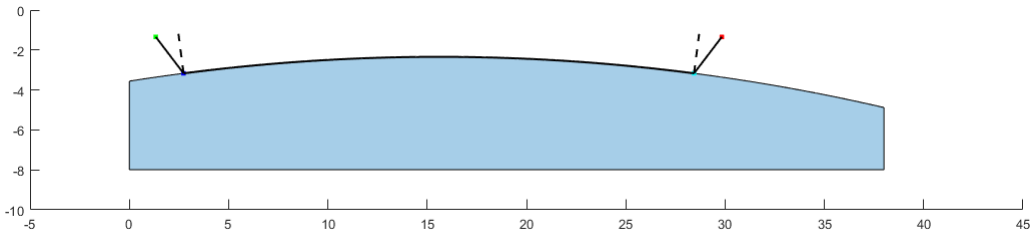

Figure 2.4: An example of a head wave path calculated using the assumption that the critical angle is the same as for a flat bone, and the head wave travels along the surface (type 1). The dotted lines are the normals to the surface.

derived by considering the triangle TAC, as shown in figure 2.3. The law of sines gives:

$$\frac{\gamma}{c} = \frac{180° - \theta_c}{TC} \tag{2.8}$$

Where TC is the length of the side between T and C, and c is the radius of the semicircle. Since the angles in a triangle must sum to $180°$, we get $\gamma = \theta_c - \alpha_2$. Substituting this into our law of sines gives:

$$\alpha_2 = \frac{c(\theta_c - 180°)}{TC} + \theta_c \tag{2.9}$$

A similar derivation for B gives $\beta_2 = \alpha_2$. From these values α and β can be calculated, and thus the position of A and B and the travel time of the head wave can be found.

2.1.3. Numerical method for arbitrary geometry

In this section we will discuss a method to find the trajectory of the head wave for arbitrary geometries. Again the assumption is used that the head wave enters and exits the bone at the critical angle. The geometry of the bone is given as a polygon (more specifically, a list of vertices). For each side of the polygon, the computer program determines the position of the point A, if it would lie on (the infinite extension of) this side. This can be done, since the angle between the head wave and the normal of the side is known: this is the critical angle. For most of the sides, this calculated position lies outside of the side. However, if it lies inside the line segment, the position of A is found. The procedure is repeated for B. An example of a path found in this way is shown in figure 2.4.

2.2. Computer simulation of the measurements

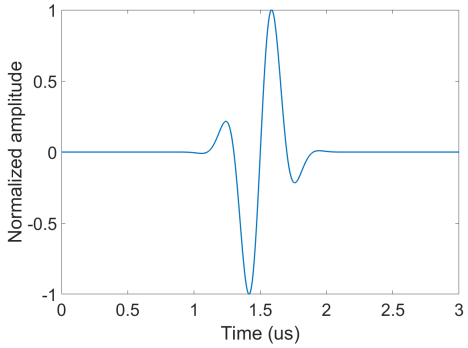

Figure 2.5: Plot of the source signal used to excite the transmitter. The horizontal axis represents the time in μs while the vertical axis represents the normalised amplitude.

The SimSonic2D program is used to perform the computer simulations. The required input files are created using a Matlab script.

The simulation setup assumes that the bone is a two-dimensional geometry immersed in soft tissue, as shown in figure 2.1. Again soft tissue is modelled as water, as they have similar acoustic properties.

Other properties of the simulation, such as the CFL coefficient and the simulation length, are given in table 2.1. The SimSonic2D simulation program automatically selects a spatial time step based on these properties.

The properties of the bone are based on those of the cortical bone in a human skull. This cortical bone can be appropriately modelled by a plate with a longitudinal speed of sound of 3 mm/μs.

First the Matlab script calculates the longitudinal sound wavelength in the bone:

$$\lambda_{bone} = \frac{v_{bone,longitudinal}}{f_0} \tag{2.10}$$

Where f_0 is the center frequency of the probe used in the experiment. For this project, a Philips P4-1 Cardiac Sector Probe was considered. This probe was chosen because it is already used for the transcranial imaging itself. Measuring the speed of sound in the skull using the same probe can thus save resources. The properties of the P4-1 probe can be found in table 2.2.

All emitters and receivers are positioned at least $2\lambda_{bone}$ away from the edge of the simulation. Furthermore there is a margin of the same size underneath the bottom edge of the bone
To simulate the measurements taken by a P4-1 probe, a transmitter and 95 receivers are added to the simulation. These have the properties of the P4-1 probe given in table 2.2.
The Simsonic program characterises materials according to their density and their stress tensors. To turn the lateral and shear speed of sound of the bone into the stress tensor, the following equations are used:

$$\begin{aligned} C_{11} = C_{22} &= v^2_{bone,longitudinal} \cdot \rho_{bone} \\ C_{12} &= v^2_{bone,shear} \cdot \rho_{bone} \\ C_{66} &= \frac{1}{2} \cdot (C_{11} - C_{12}) \end{aligned} \tag{2.11}$$

For the soft tissue the stress tensor values for water are used:

$$C_{11} = C_{22} = C_{12} = 2.25 \text{ GPa, and } C_{66} = 0$$

The transmitter was set to produce a Gaussian pulse with the same center frequency as the probe, starting at $t = 1.5$ μs. This transmitter excited the vertical velocity of the medium according to this signal. A plot of this pulse can be seen in figure 2.5. The receivers were set to record the velocity of the medium in the vertical direction at every point in time.

Maximum speed	3 mm/μs
Simulation length	17 μs
CFL coefficient	0.99
$v_{bone,longitudinal}$	3 mm/μs
$v_{bone,shear}$	0.954 mm/μs
ρ_{water}	1.0 mg/mm^3
ρ_{bone}	1.450 mg/mm^3

Table 2.1: Parameters of the simulation. The maximum speed is used by the simulation program to determine the dt automatically. ρ_{bone} and ρ_{water} are the densities of cortical bone and water, respectively.

Center frequency	2.5 MHz
Bandwidth	1.5 - 3.5 MHz
Transducer width	0.24 mm
Transducer pitch	0.2873 mm
Number of transmitters	1
Number of receivers	95

Table 2.2: Parameters of the P4-1 probe used in these simulations.

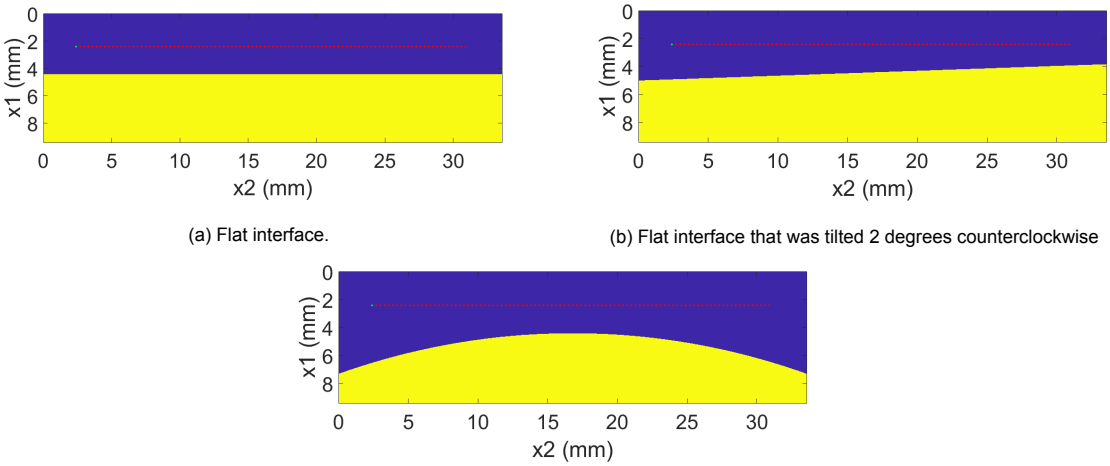

(a) Flat interface.

(b) Flat interface that was tilted 2 degrees counterclockwise

(c) Semicircular interface

Figure 2.6: Plot of the simulation setup for single interfaces with different geometries. The blue and yellow regions represent the soft tissue and the bone, respectively. The green dot is the location of an emitter, while the red dots are receivers. To obtain the reverse transmission data for the bidirectional method, this simulation was repeated with the transmitter being the far right element of the array.

In the computer simulations, the new trajectory-based method is compared with the current bidirectional technique. To this end, simulations are made on three geometries with a single interface. The first geometry consists of a straight interface between a 2 mm thick layer of water and a 5 mm thick layer of bone. The second geometry is similar to the first geometry, but the interface is rotated 2 degrees counterclockwise around its midpoint. For the third geometry, the interface is replaced by a semicircle with 50 mm radius. A last set of simulations is done on a semicircle with a 40 mm radius. The top of this circle is on the original bone-water interface (so 2 mm from the probe) and horizontally underneath the middle of the transmitter-receiver array. Pictures of these geometries are shown in figure 2.6. Based on the conclusions of a convergence test, all simulations use a spatial step size of 5 μm. More details about the convergence test can be found in appendix B. To be able to apply the bidirectional method, simulations are made both with the transmitter on the far left and the far right of the transducer array. After these simulations are done, both the trajectory-based method and the bidirectional method are applied to the results. The velocities necessary for the bidirectional method are obtained by applying the semblance method for a straight interface. More information on the semblance method is given in section 2.3.

2.3. Data analysis of the simulation results

The results of these simulations are analysed in two ways. The first way is to use the conventional straight-line semblance method to find the speed of sound for forward and backward propagation. The bidirectional correction is then applied to get a final result. The second way is to only consider the forward propagation, but to consider a trajectory that is not a straight line. By the methods described in the first section, these trajectories can be found for different geometries. Finding the trajectories corresponding to different velocities thus gives the test lines that can be used for the semblance calculation.

First, for both methods, the data is masked. This is necessary since the receivers do not only pick up the head wave, but also the direct wave and reflected waves. For this project, a simple mask is used. First, the x-t diagrams are inspected, and the direct wave is marked. The head wave can then be seen as the first signal that “overtakes” this direct wave, and arrives earlier after a few receivers. It is then also noted at which point the head wave starts interfering with other waves. For a certain region of x-values, the head wave is clearly the first arriving signal, and there is no interference. This region of x-values is then chosen as the mask, and all data outside this region is deleted. In the case of a semicircular bone, this region is the x-values from 12 to 20 mm. An example of an x-t diagram with this mask is shown in figure 3.6. The green lines correspond to the mask.

After this masking, the two methods start to differ. First, the straight line semblance for the bidirectional method is explained. For this semblance, the first 10 time samples are thrown away, to prevent reflections off the simulation wall from being considered. Now a peak-finding method is used on the data of the first remaining receiver, to find a point that lies on the head wave. This is complicated by the fact that the head wave consists of multiple peaks, that may be negative as well. Furthermore, peaks corresponding to the direct or reflected waves must not be considered. To do this, we do some post-processing of the peak data. First a standard peak-finding method is used to find all peaks in the first 10μs of (the absolute value of) the data. This excludes the reflected waves, which arrive long after 10μs. Next, all peaks that are bigger than 0.03 are removed. This is done so that the peaks corresponding to the direct wave, which is much bigger than the head wave, are ignored. Finally, the remaining peak of maximum size is selected. This is done so that a peak is found that corresponds to the middle of the head wave, and one of the other peaks associated with the head wave. In the standard peak-finding method, a minimum peak prominence of 0.01 was required to avoid spurious peaks from being considered. Having found this peak, we have found a point on the head wave. The coordinates of this point are called x_{int} and t_{int}.

Since the speed of sound in the bones was set to 3 mm/μs, the speed of the head wave is expected to be between $V_- = 2.5$ and $V_+ = 3.5$ mm/μs. 1001 equally spaced V_{test} in $[V_-, V_+]$ are generated using $V_{test,i} = V_- + i \cdot (V_+ - V_-)\,/1000$ (where i runs from 0 to 1000). For each V_{test}, a test line is created that has slope V_{test} and goes trough x_{int} and t_{int}. The formula of this test line is $t_{center}(x) = t_{int} + x/V_{test}$. Since the simulation only has results where we positioned receivers, this can be rewritten to $t_{center}(i) = t_{center}(i \cdot p)$, where p is the pitch between the transducers.

For each V_{test} the semblance S is then calculated using:

$$S = \frac{\sum_{j=\lceil t_{center}-W/2 \rceil}^{\lfloor t_{center}+W/2 \rfloor} \left(\sum_{i=1}^{N_{rec}} Sig(i,j) \right)^2}{N_{rec} \sum_{j=\lceil t_{center}-W/2 \rceil}^{\lfloor t_{center}+W/2 \rfloor} \sum_{i=1}^{N_{rec}} \left(Sig(i,j) \right)^2} \tag{2.12}$$

Where N_{rec} is the number of receivers and W is the size of the time window. Since $W = 1$, the sum is only over the trajectory itself and thus the middle sum disappears. The semblance is then plotted as a function of V_{test}. The V_{test} with the highest semblance is then assumed to be the velocity of the head wave, as it fits the received signals the best. By repeating this process for the forward and the reverse transmission, the bidirectional correction formula (formula 1.1) can be used.

The trajectory-based method follows a slightly different procedure. The peak-finding process is skipped, since x_{int} and t_{int} are not used. V_{test} are calculated in the same way. The trajectory $t_{center}(x)$ is found using one of the methods described in the first section of this chapter, by moving the receiver to position x and changing the speed of sound to V_{test}. The semblance is then calculated in the same way, and the velocity with the highest semblance is given as the final result. Since the trajectory-based method already considers the geometry, it is not necessary to consider the reverse transmission case or apply bidirectional correction. More background information on the semblance method is given in the introduction.

3

Results

3.1. Comparison with bidirectional method

This section will discuss the speed of sound found by the different methods on the different geometries. An interesting result is that applying an interpolation to the data set does not always improve the result of these methods. For the flat and tilted interface, interpolation had no effect on either of the methods. For the semicircular interface, interpolation slightly improved the result of the bidirectional method, but gave a worse result for the trajectory-based method. These surprising results are further explained in the discussion chapter. A more detailed examination of each of the simulations, including some x-t and semblance plots, is done below.

3.1.1. Flat interface

Simulation	Velocity (mm/μs)	error (%)
Forward velocity	2.996	
Reverse velocity	2.996	
Bidirectional method	2.996	0.13
Trajectory-based method	2.991	0.30

Table 3.1: Speed of sound (in mm/μs) found by the bidirectional and the trajectory-based method for the flat interface (as shown in figure 2.6a). No interpolation was applied. The percentage difference to the true speed of sound of these simulations is also shown. For all of these measurements this true speed of sound was 3 mm/μs. The result for the bidirectional method is calculated by applying the bidirectional correction formula (formula 1.1) to the forward and reverse velocity.

The velocities found by the different methods for the flat interface simulation are given in table 3.1. For these simulations, It can be seen that the forward and reverse velocity are the same. This makes sense, since the flat bone is symmetric around the vertical axis. In this case, the bidirectional correction formula (formula 1.1) also gives this value, which results in a 0.13% error. The trajectory-based method has a slightly higher error of 0.3%.

The x-t diagram for the forward transmission is given in figure 3.1. The x-t diagram for the reverse transmission is an exact mirror image of this figure, and the x-t diagram for the trajectory-based method is identical to that for forward transmission. This makes sense, since in this case the bone actually has a flat interface, and thus the correct trajectory is a straight line. A masking of x between 12 and 28.5 mm (the last receiver) was used for these simulations after manually looking for interference with the head wave. In these figures, it can be seen that the maximum semblance trajectory (the orange line) fits down the middle of the wavefront of the head wave. Therefore both methods correctly estimate the speed of sound of the head wave.

The semblance plots for this simulation are given in figures 3.2a and 3.2b. The semblance plot for the reverse transmission of the bidirectional method is omitted, since it is an exact mirror image of that for the forward transmission. One interesting result is that the semblance plot for the bidirectional

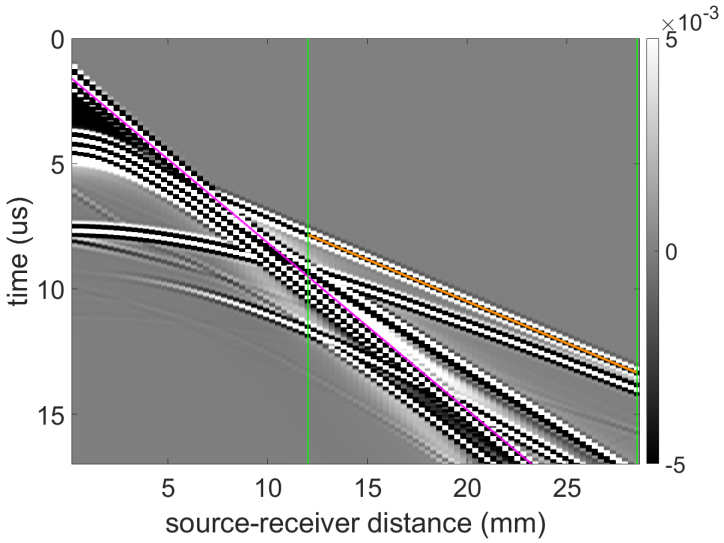

Figure 3.1: An x-t diagram for the straight interface geometry shown in figure 2.6a. The speed of sound in the medium is 3 mm/μs, and excitation signal has a frequency of 2.5 MHz. The brightness at each point of the graph represents the vertical speed of the medium. The pink line corresponds to the direct wave. The green lines represent the outer limits of the mask, while the orange line corresponds to the trajectory found by the semblance method.

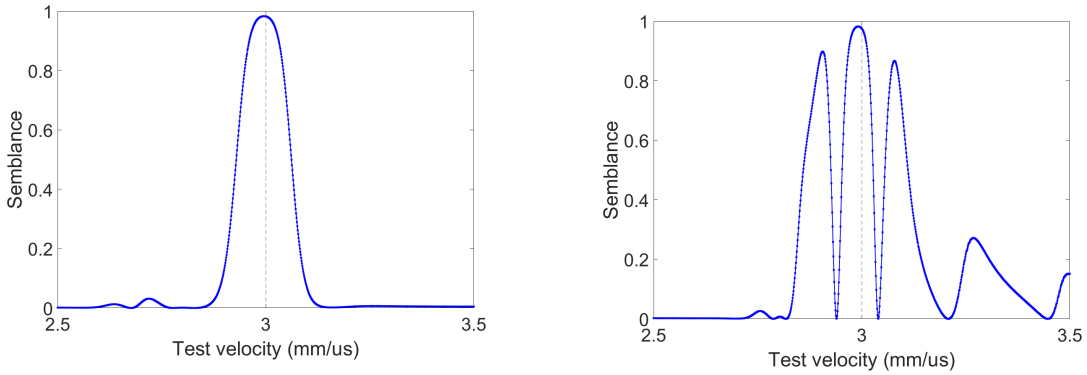

(a) Bidirectional method: Forward transmission

(b) Trajectory-based method

Figure 3.2: Semblance plots for the straight interface geometry shown in figure 2.6a. The vertical axis is the semblance while the horizontal axis corresponds to the test velocity. For these plots the true velocity of the bone was 3 mm/μs, indicated by the dotted line. The semblance plot for the reverse transmission of the bidirectional method is omitted, since it is an exact mirror image of that for the forward transmission.

method is much smoother than that for the trajectory-based method. Nevertheless, both semblance plots clearly have a highest peak. Furthermore, this peak is close to the true speed of sound.

Applying the cubic interpolation does not change the results. Both the speed of sound, the fit on the x-t diagram and the semblance plots are identical. The only difference is that the actual data becomes more smooth, as seen in figure 3.3. This is a result of the interpolation itself, so the bidirectional method and the trajectory-based method are not affected at all by the interpolation.

3.1.2. Tilted interface

The velocities found by the different methods for the tilted interface simulation are given in table 3.2. From this table, we see that the forward velocity overestimates the speed of sound, while the reverse velocity underestimates it. This makes sense, since a tilted bone is no longer symmetric in the vertical axis and thus there is a real difference between forward and reverse propagation. The bidirectional correction formula (formula 1.1) is applied to these velocities with $\alpha = 2$ degrees, since that is the angle of this interface. This corrected velocity corresponds very well with the true speed of sound, having

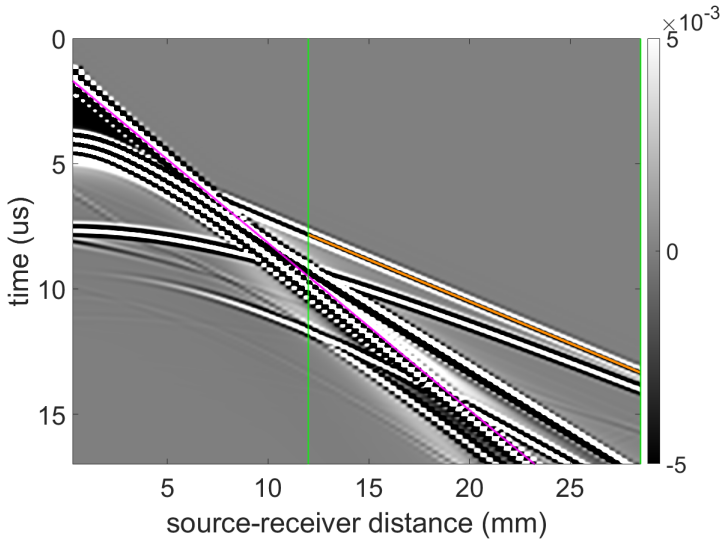

Figure 3.3: An x-t diagram for the straight interface geometry shown in figure 2.6a. A cubic interpolation with a refinement of 4 was applied. The speed of sound in the medium is 3 mm/μs, and excitation signal has a frequency of 2.5 MHz. The brightness at each point of the graph represents the vertical speed of the medium. The pink line corresponds to the direct wave. The green lines represent the outer limits of the mask, while the orange line corresponds to the trajectory found by the semblance method.

Simulation	Velocity (mm/μs)	error (%)
Forward velocity	3.189	
Reverse velocity	2.827	
Bidirectional method	2.995	0.16
Trajectory-based method	2.993	0.23

Table 3.2: Speed of sound (in mm/μs) found by the bidirectional and the trajectory-based method for the 2 degrees tilted interface (as shown in figure 2.6b). No interpolation was applied. The percentage difference to the true speed of sound of these simulations is also shown. For all of these measurements this true speed of sound was 3 mm/μs. The result for the bidirectional method is calculated by applying the bidirectional correction formula (formula 1.1) to the forward and reverse velocity.

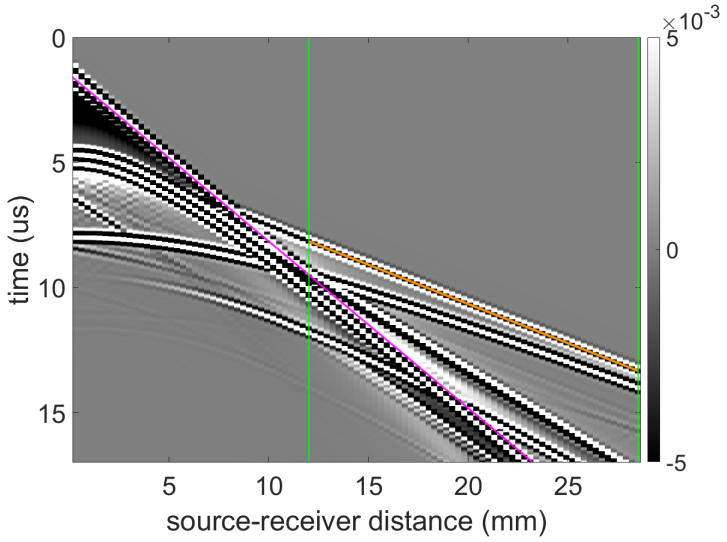

Figure 3.4: An x-t diagram for the tilted interface geometry shown in figure 2.6b. The tilt is exactly 2 degrees with respect to the horizontal. The speed of sound in the medium is 3 mm/μs, and excitation signal has a frequency of 2.5 MHz. The brightness at each point of the graph represents the vertical speed of the medium. The pink line corresponds to the direct wave. The green lines represent the outer limits of the mask, while the orange line corresponds to the trajectory found by the semblance method.

only a 0.16% error. The trajectory-based method again has a slightly higher error, at 0.23%.

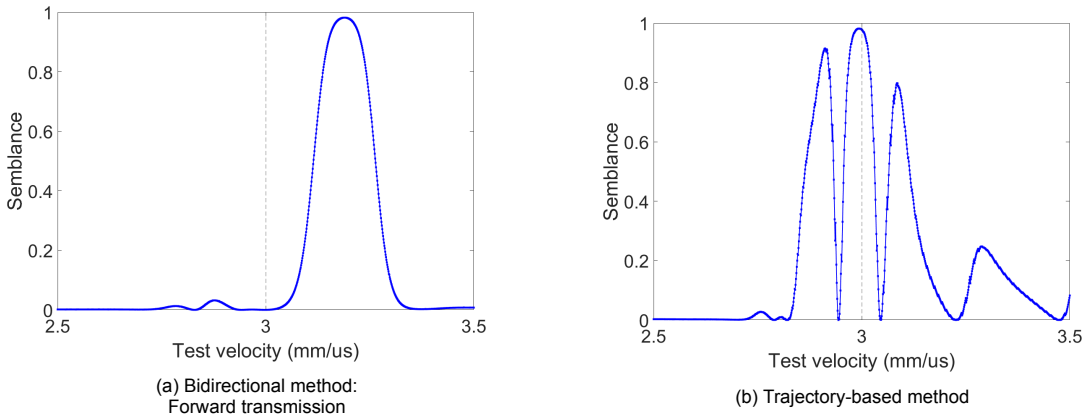

(a) Bidirectional method: Forward transmission

(b) Trajectory-based method

Figure 3.5: Semblance plots for the tilted interface geometry shown in figure 2.6b. The tilt is exactly 2 degrees with respect to the horizontal. The vertical axis is the semblance while the horizontal axis corresponds to the test velocity. For these plots the true velocity of the bone was 3 mm/μs, indicated by the dotted line. The semblance plot for the reverse transmission of the bidirectional method is omitted, since it is similar to that for the forward transmission.

The x-t diagram for the forward transmission on this tilted interface is given in figure 3.4. After a manual inspection of this diagram, the mask is again chosen to be x between 12 and 28.5 mm. It can again be seen that the maximum semblance trajectory fits down the middle of the head wave wavefront. The x-t diagram for the trajectory-based method is identical, since the correct trajectory for the head wave is again a straight line. The x-t diagram for the reverse transmission is almost identical: though the wavefront of the head wave travels at a different angle, the maximum semblance trajectory fits down the middle of it. Therefore these diagrams are omitted from this report. The semblance plots for this simulation are given in figures 3.5a and 3.5b. The semblance plot for the reverse transmission of the bidirectional method is omitted, since it looks identical to that for the forward transmission, except for the fact that the peak is at 2.827 mm/μs instead of 3.189 mm/μs. Again there is a clear peak near the true speed of sound for both methods. Furthermore, the semblance plot for the trajectory-based method is much rougher than that for the bidirectional method.

Similarly to the case of the flat interface, applying the interpolation does not change anything. While the x-t diagrams themselves look smoother, the maximum semblance trajectories and thus the calculated velocities do not change. Furthermore, the semblance plots are the same as for the uninterpolated case.

3.1.3. Semicircular interface

Simulation	Velocity (mm/μs)	error (%)
Forward velocity	2.937	
Reverse velocity	2.944	
Bidirectional method	2.940	2.00
Trajectory-based method	2.997	0.10

Table 3.3: Speed of sound (in mm/μs) found by the bidirectional and the trajectory-based method for the semicircular interface with a 50 mm radius (as shown in figure 2.6c). No interpolation was applied. The percentage difference to the true speed of sound of these simulations is also shown. For all of these measurements this true speed of sound was 3 mm/μs. The result for the bidirectional method is calculated by applying the bidirectional correction formula (formula 1.1) to the forward and reverse velocity.

The velocities found by the different methods for the 50 mm radius semicircular interface simulation are given in table 3.3. We can now see that the bidirectional method begins to break down: both the forward and reverse velocity underestimate the speed of sound. Since the semicircle is horizontally centred underneath the probe, the best fitting straight line to the geometry is horizontal. Therefore, the bidirectional correction formula (formula 1.1) is applied to these velocities with $\alpha = 0$ degrees. The resulting corrected velocity has an error of 2%. This large error is to be expected, since the bidirectional method has been developed to compensate for angled interfaces, and not for other geometries. The

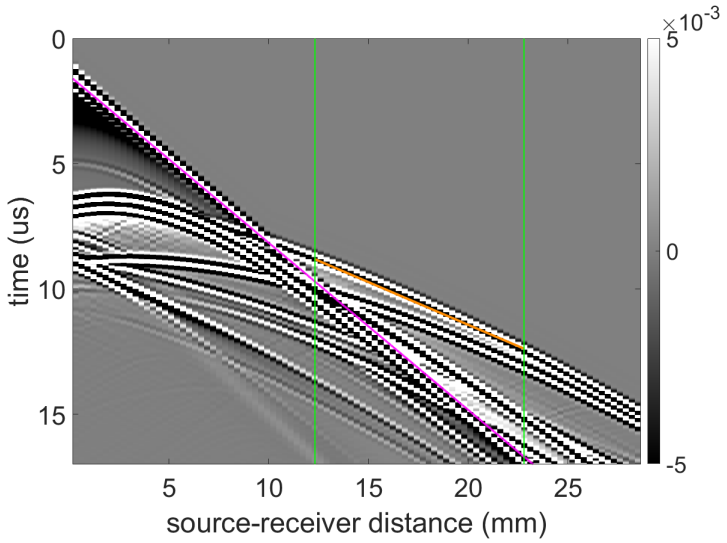

Figure 3.6: An x-t diagram for the semicircular interface geometry shown in figure 2.6c. The radius of the semicircle is 50 mm. The speed of sound in the medium is 3 mm/μs, and excitation signal has a frequency of 2.5 MHz. The brightness at each point of the graph represents the vertical speed of the medium. The pink line corresponds to the direct wave. The green lines represent the outer limits of the mask, while the orange line corresponds to the trajectory found by the semblance method.

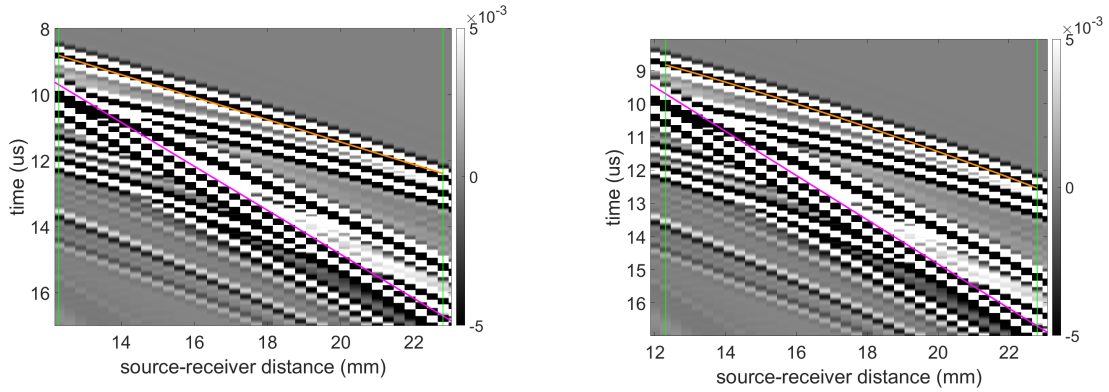

(a) Bidirectional method: Forward transmission

(b) Trajectory-based method

Figure 3.7: Zoomed-in versions of the x-t diagram for the semicircular interface geometry shown in figure 2.6c, for different methods. The radius of the semicircle is 50 mm. The speed of sound in the medium is 3 mm/μs, and excitation signal has a frequency of 2.5 MHz. The brightness at each point of the graph represents the vertical speed of the medium. The pink line corresponds to the direct wave. The green lines represent the outer limits of the mask, while the orange line corresponds to the trajectory found by the semblance method.

trajectory-based method, on the other hand, is intended to be used for any kind of geometry. Indeed this method gives a much better result: this has an error of only 0.1%. In the discussion of the semblance plots we will see that this extremely good result is mostly due to coincidence, but that in general the trajectory-based method should still perform much better than the bidirectional method.

The x-t diagram for the forward transmission on this semicircular interface is given in figure 3.6. After a manual inspection of this diagram, the mask is chosen to be x between 12.3 and 22.8 mm. For the semicircular interface the trajectory of the head wave becomes curved. Therefore, the straight line trajectories used by the bidirectional method can no longer accurately fit to the head wave. An example of this is given in figures 3.7a and 3.7b. These are versions of the x-t diagram that are zoomed in on the masked area. In these images, it can clearly be seen that the maximum semblance trajectory (i.e. the orange line) of the trajectory-based method is a much better fit to the data than the one found by the bidirectional method. The situation is similar for the reverse propagation, and thus it is omitted.

The semblance plots for this simulation are given in figures 3.8a and 3.8b. The semblance plot for the

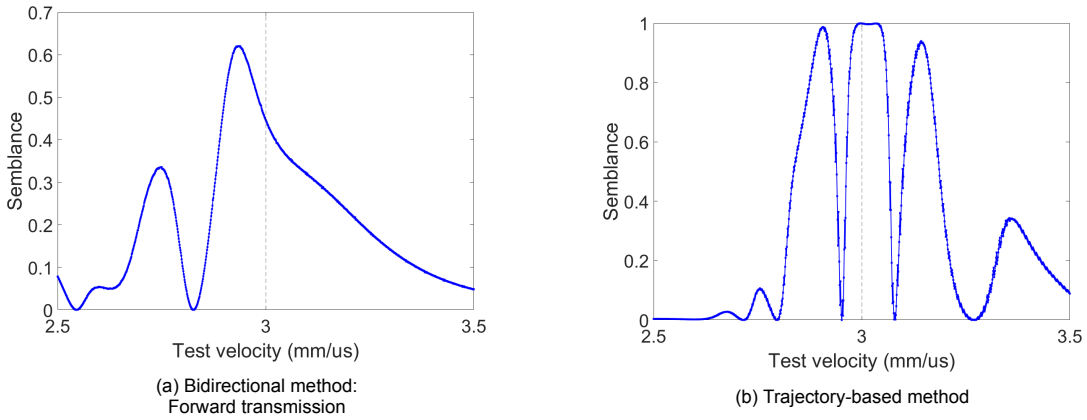

(a) Bidirectional method: Forward transmission

(b) Trajectory-based method

Figure 3.8: Semblance plots for the semicircular interface geometry shown in figure 2.6c. The semicircle has a radius of 50 mm. The vertical axis is the semblance while the horizontal axis corresponds to the test velocity. For these plots the true velocity of the bone was 3 mm/μs, indicated by the dotted line. The semblance plot for the reverse transmission of the bidirectional method is omitted, since it is similar to that for the forward transmission.

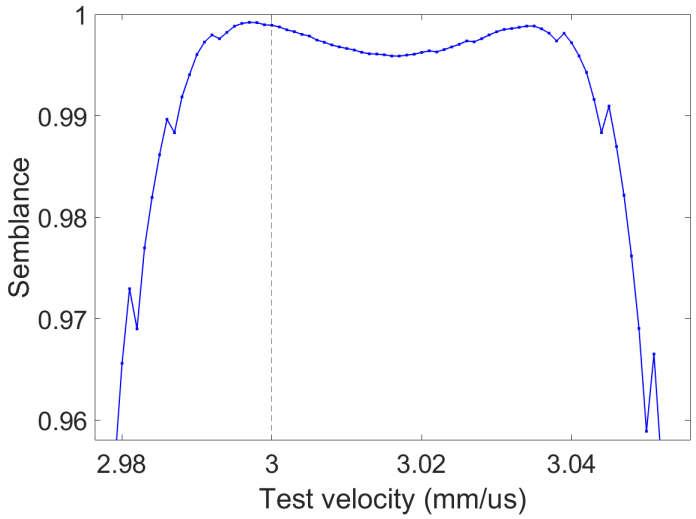

Figure 3.9: Zoomed version of the semblance plot for the semicircular interface geometry shown in figure 2.6c. The semicircle has a radius of 50 mm. This plot corresponds to the trajectory-based method. The vertical axis is the semblance while the horizontal axis corresponds to the test velocity. For these plots the true velocity of the bone was 3 mm/μs, indicated by the dotted line.

reverse transmission of the bidirectional method is omitted, since this is a mirror image of that for the forward transmission. It can be seen that the semblance plot for the bidirectional method is now no longer a single peak. Instead, it consists of multiple peaks, with smaller amplitudes than for the other geometries. This is probably a result of the straight line semblance no longer being able to correctly fit to the curved head wave trajectory. The semblance plot for the trajectory-based method looks similar to that of the other geometries, but now the peak in the middle has a flat top. Furthermore, looking at this flat-topped peak we expect the maximum semblance to be attained somewhere in the middle of this flat top, at around 3.015 mm/μs. Instead, as we have seen in the table, it is actually attained for 2.997 mm/μs. To explain this, figure 3.9 shows a version of the semblance plot for the trajectory-based method, zoomed in on the top of this middle peak. In this figure, we see that the flat top of the middle peak is actually not completely flat. We see that it has two high points: one happens to be at 2.997 mm/μs. and the other is at around 3.035 mm/μs. If this other maximum were to have been slightly bigger than the other maximum, the trajectory-based method would have had an error of 1.16%. This is however, not a fair comparison. The real result of the trajectory-based method would be in the middle of these two maxima, as there are not two separate peaks, but rather one peak that has a mostly flat

top. This would mean that the result of the trajectory-based method should have been 3.015 mm/μs, giving an error of 0.5%. While this is not as good of a result as we initially have seen, it is still a great improvement compared to the 2% error given by the bidirectional method. In the discussion chapter, we will mention methods on how to compensate for the flat peaks in semblance plots.

Simulation	Velocity (mm/μs)	error (%)
Forward velocity	2.937	
Reverse velocity	2.945	
Bidirectional method	2.941	1.97
Trajectory-based method	3.009	0.3

Table 3.4: Speed of sound (in mm/μs) found by the bidirectional and the trajectory-based method for the 50mm radius semicircular interface (as shown in figure 2.6c). A cubic interpolation with a refinement of 4 was applied. The percentage difference to the true speed of sound of these simulations is also shown. For all of these measurements this true speed of sound was 3 mm/μs. The result for the bidirectional method is calculated by applying the bidirectional correction formula (formula 1.1) to the forward and reverse velocity.

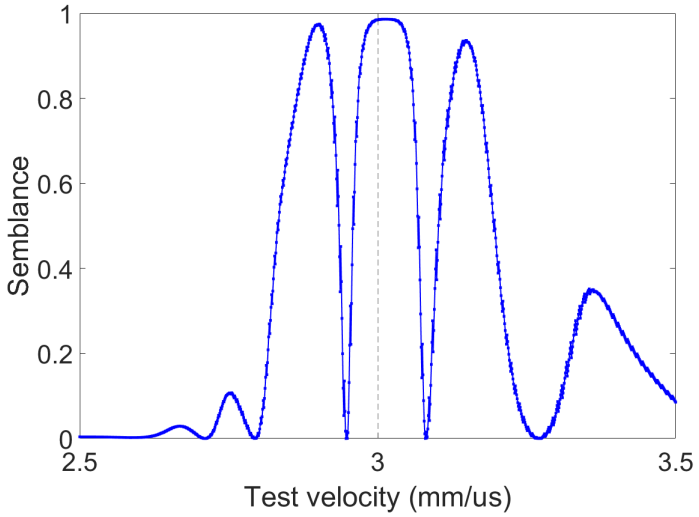

Figure 3.10: The semblance plot for the semicircular interface geometry shown in figure 2.6c. The semicircle has a radius of 50 mm. A cubic interpolation with a refinement of 4 has been applied to the data before the semblance method was applied. This plot corresponds to the trajectory-based method. The vertical axis is the semblance while the horizontal axis corresponds to the test velocity. For these plots the true velocity of the bone was 3 mm/μs, indicated by the dotted line.

Results for the semicircular interface with a 50 mm radius and with interpolation are given in table 3.4. The results for the bidirectional method are almost exactly the same. The trajectory-based method, on the other hand, produces a higher error of 0.3%. The semblance plot is shown in figure 3.10, and a zoomed version is shown in figure 3.11. The middle peak is still flat, but at a first glance it does not seem to split into multiple peaks. Unfortunately, the middle of the peak is still below the sides: the peak is actually centred around 3.015 mm/μs (0.5% error). Even though it is less clear than in the uninterpolated case, the flat peak still causes ambiguity when determining the speed of sound.

Simulation	Velocity (mm/μs)	error (%)
Forward velocity	2.735	
Reverse velocity	2.740	
Bidirectional method	2.737	8.7
Trajectory-based method	3.047	1.6

Table 3.5: Speed of sound (in mm/μs) found by the bidirectional and the trajectory-based method for the 40mm radius semicircular interface (as shown in figure 2.6c, but with a different radius). The percentage difference to the true speed of sound of these simulations is also shown. For all of these measurements this true speed of sound was 3 mm/μs. The result for the bidirectional method is calculated by applying the bidirectional correction formula (formula 1.1) to the forward and reverse velocity.

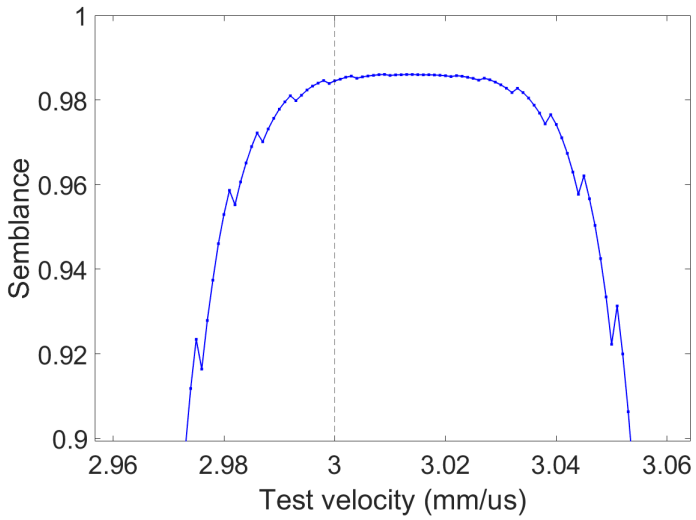

Figure 3.11: Zoomed version of the semblance plot for the semicircular interface geometry shown in figure 2.6c. The semicircle has a radius of 50 mm. A cubic interpolation with a refinement of 4 has been applied to the data before the semblance method was applied. This plot corresponds to the trajectory-based method. The vertical axis is the semblance while the horizontal axis corresponds to the test velocity. For these plots the true velocity of the bone was 3 mm/μs, indicated by the dotted line.

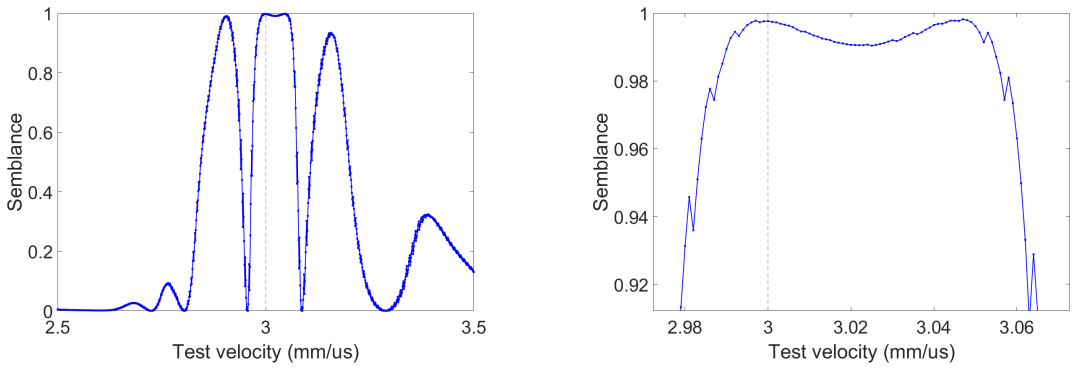

(a) Original (b) Zoomed

Figure 3.12: Semblance plots for the semicircular interface geometry shown in figure 2.6c. The semicircle has a radius of 40 mm. Both plots correspond to the trajectory-based method. The vertical axis is the semblance while the horizontal axis corresponds to the test velocity. For these plots the true velocity of the bone was 3 mm/μs, indicated by the dotted line.

Results for the simulation on a semicircular bone with a 40 mm radius and no interpolation are given in table 3.5. It can be seen that in this situation the trajectory-based method again has a lower error than the bidirectional method. The trajectory-based method still has a relatively large error of 1.6%.The semblance plots are shown in figures 3.12a and 3.12b. The situation is very similar to that of the 50 mm radius semicircle. There is also a flat peak that split into multiple peaks. However, now the peak that is furthest from the true value happens to be larger, which causes the large error.

The results for the interpolated case can be seen in table 3.6. It can be seen that the interpolation improves the results for both the bidirectional method and the trajectory-based method. The trajectory-based method still has a significantly lower error of 0.43%, compared to 1.9% for the bidirectional method. The semblance plots can be seen in figures 3.13a and 3.13b. Like in the case of the 50 mm radius semicircle, there is one peak, but with a center that is lower than the sides.

Simulation	Velocity (mm/μs)	error (%)
Forward velocity	2.938	
Reverse velocity	2.950	
Bidirectional method	2.944	1.9
Trajectory-based method	3.013	0.43

Table 3.6: Speed of sound (in mm/μs) found by the bidirectional and the trajectory-based method for the 40mm radius semicircular interface (as shown in figure 2.6c, but with a different radius). A cubic interpolation with a refinement of 4 was applied. The percentage difference to the true speed of sound of these simulations is also shown. For all of these measurements this true speed of sound was 3 mm/μs. The result for the bidirectional method is calculated by applying the bidirectional correction formula (formula 1.1) to the forward and reverse velocity.

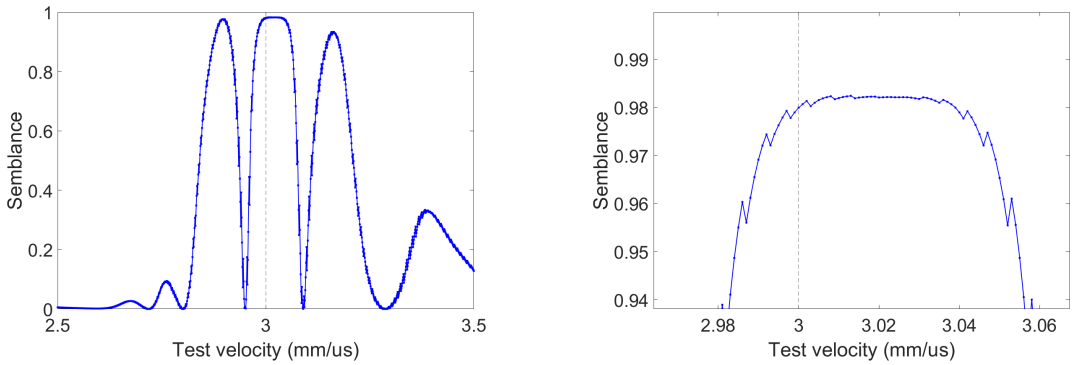

(a) Original (b) Zoomed

Figure 3.13: Semblance plots for the semicircular interface geometry shown in figure 2.6c. The semicircle has a radius of 40 mm. Both plots correspond to the trajectory-based method. A cubic interpolation with a refinement of 4 has been applied to the data before the semblance method was applied. The vertical axis is the semblance while the horizontal axis corresponds to the test velocity. For these plots the true velocity of the bone was 3 mm/μs, indicated by the dotted line.

4

Discussion

The results of our comparison of the trajectory-based method and the bidirectional method mostly match what we expected. The bidirectional method works perfectly for the flat and tilted interface (0.13, 0.16% error) since it is designed to compensate for an angle between the bone and the receiver. It breaks down for a semicircular interface (1.97 to 8.7% error), since a semicircular geometry is really different from a flat interface that is tilted with respect to the receiver. Our proposed trajectory-based method performs slightly worse than the bidirectional method for the flat and tilted interface (0.23, 0.3% error) but works much better for the semicircular interface (0.1, to 0.4% error). This too makes sense, as our method has been designed to work with geometries that are not simply flat or tilted. The trajectory-based method only has a high error for the 40 mm semicircular interface without interpolation (1.6%) which is still less than that for the bidirectional method. The cause of this error is discussed below.

The fact that the error is slightly higher for the trajectory-based method on the flat and tilted interfaces may be the result from the additional assumptions that the trajectory-based method makes. The bidirectional method only assumes that the wavefront corresponding to the head wave travels along a straight line, and uses a peak-finding method to find a point on this line. On the other hand, the trajectory-based method considers the geometry of the bone, the precise location of the transmitters and receivers and the time at which the transmission starts. Small errors in these assumptions might cause the trajectories corresponding to different velocities to be wrong and thus cause an error in the calculated velocity. While in this project these values come directly from the simulation, there may still be rounding errors or imperfections in the simulation method that cause these values to be less accurate. Furthermore, since the trajectories are found using a numerical method, these trajectories can also be slightly off due to rounding errors.

Another unexpected result is that interpolating the data in the x-t diagram does not always improve the calculated velocities. Indeed, for the flat and tilted interface interpolation does not change the results at all. For the semicircular interface, interpolation slightly improves the result for the bidirectional method. For the bidirectional method the result is worse for the 50 mm radius, but better for the 40 mm radius. In the next paragraph we will talk about the weird shape of the semblance plot for the trajectory-based method: this will provide an explanation why interpolation could cause a worse result. This does not, however, explain why interpolation often only minimally improves the result. The original purpose of the interpolation was to give more points for the trajectory to be checked against the data, and thus cause the correct trajectory to have a higher semblance. Apparently such an effect does not occur, this could be because interpolation does not actually provide new data, but attempts to guess the data at various points given the original data. These guesses are apparently made in such a way that they do not significantly impact the methods used in this report.

In the results section, the semblance plot of the trajectory-based method was discussed. While this method gave a very accurate result for the semicircular bone, this result was only a consequence of an irregular peak in the semblance plot. This peak has a flat top, with two local maxima on both sides. An example of such a peak can be seen in figure 3.9. Small differences in the simulation,

such as using a different interpolation, could cause one peak to become higher than the other, and thus lead to an incorrect result. This can be seen for the results of the uninterpolated 40 mm radius semicircular interface. An interesting observation is that these flat peaks do not occur for the flat or tilted interface. We therefore conclude that this must be a result of the trajectories along which the semblance is calculated not being straight lines. Perhaps this is for the same reason as the higher error of the trajectory based method: the input variables not being exactly correct. Rounding errors in the input data could cause the trajectories along which the semblance is calculated to have a slightly different curvature than the real trajectory. This would prevent a single velocity from fitting the data perfectly, and thus lead to a flat peak in the semblance plot. One method to solve this problem would be to check if there are two peaks close to each other, and then that the velocity to be the average position of these two peaks. These peaks also seem to disappear when interpolation is applied to the received data, but the resulting peak is still flat and can still cause the same problems, since the center of the peak is lower than the sides. It is possible that a stronger interpolation, or a different type of interpolation, could fix these issues.

The possibility of flat peaks is not the only difference between the semblance plots of the bidirectional and the trajectory-based method. As can be seen in figures 3.5a and 3.5b, the semblance plot for the bidirectional method consists of one clear peak, while that for the trajectory-based method consists of three large peaks. One explanation for this could be the shape of the wavefront of the head wave. As can be seen in figure 3.7a, the head wave consists of three parallel contributions: a black negative peak in between two positive white peaks. This is not a problem for the bidirectional method, since a peak-finding method is used to find a point on the negative peak in the middle. All the test trajectories for the head wave then go trough this point, making it impossible to fit to one of the positive peaks on the outside. For the trajectory-based method, on the other hand, no such peak-finding is used. Instead, the trajectories are based directly on the physical situation. When observing the trajectories corresponding to different velocities, it can be seen that changing the velocity not only changes the shape of the trajectory, but also translates it along the time axis. This is because in the physical model used in the trajectory-based method, the head wave also propagates for some time before hitting the first receiver (that was left after masking). This translation could cause an approximate fit to one of the positive peaks on the outside of the head wave, but more research is needed to confirm this.

One possible solution for this rough semblance plot is to increase the window size for the semblance method. Earlier versions of this report also examined results for a window sizes of 51 and 2 units in the time domain. In these simulations, the semblance plot for the trajectory-based method still contains three different peaks, but the troughs in between them are much smaller. Further research could examine if an appropriate window size could aid in creating a more unambiguous semblance plot. Alternatively, further research could do away with the semblance method altogether. The trajectories found by the methods in this report can also be used in different ways. For example, after appropriate masking is done, one could use a peak-finding method to find the time at which each receiver receives the head wave. This could be done in the same way as in Lowet and Van der Perre [2]. For non-straight interfaces, the mean square error between test trajectories and these observed points could be calculated. Perhaps this method would give clearer results: further research could investigate this.

Even though this project focused on the trajectory-based method, there were also some difficulties implementing the bidirectional method. The bidirectional method uses test trajectories that have a certain velocity and go trough a point known to be on the head wave. Finding this point from the received data is not as trivial as it first seems to be. In this project, a complicated peak-finding method is used that combines a minimum prominence, a maximum arrival time and peak size, and chooses the remaining peak of maximum size.

This set of conditions came about because of two reasons. First, it is necessary to pick out precisely the middle peak corresponding to the head wave, and not the two peaks on the outside of the head wave or a peak corresponding to the direct or reflected waves. Secondly, the simulations for different interfaces led to different amplitudes of the received data. This is also the reason why a simple prominence filter did not work: the spurious peaks for the semicircular bone are bigger than the correct peak for the flat bone. Perhaps this can be fixed by using different peak-finding criteria for different simulations, or some algorithm can be found to automatically determine these criteria from the received data. This is outside the scope of this project, but could be examined by further research. Another solution is

simply to allow the bidirectional method to start from one of the outer peaks: since these peaks are also part of the wavefront of the head wave, they should follow a trajectory that is parallel to that of the middle peak. It was chosen not to allow this in this project in order to get a fair comparison with the trajectory-based method, that always follows the middle of the wavefront. Nevertheless, this is an option for further research, or in applications of the bidirectional method.

5

Conclusion

This project set out to extend the head wave method to curved bones. We have seen that for a semicircular bone, the wavefront corresponding to the head wave follows a curved path, instead of a straight line. We have proposed methods to calculate the trajectory that the head wave will follow, if the geometry and speed of sound in the bone is known. Analytic methods exist for flat and semicircular bones: for arbitrary geometries a numerical method is proposed. Qualitative examination of our results suggest that these methods are correct, as the predicted trajectories fit well to the received x-t diagrams. While we have only examined a limited set of situations, we observe that the velocity estimated by the trajectory-based method is consistently accurate, with an error of $\leq 0.43\%$ (an outlier of 1.6% was caused by ambiguity in the semblance plot). The original bidirectional method, on the other hand, performs better for straight and tilted interfaces ($\leq 0.16\%$ error) but breaks down for a semicircular bone ($\geq 1.9\%$ error). The semblance plots for the trajectory-based methods are unexpectedly rough, and this can cause problems interpreting the results. There are different approaches to solve this problem, such as increasing the window size of the semblance method, or using an alternative to the semblance method. These approaches are recommended for further research. Further research should also evaluate the trajectory-based method on other geometries and on experimental data, to confirm that it is also valid in these situations.

Appendix A: Derivation of the critical angle for a flat bone

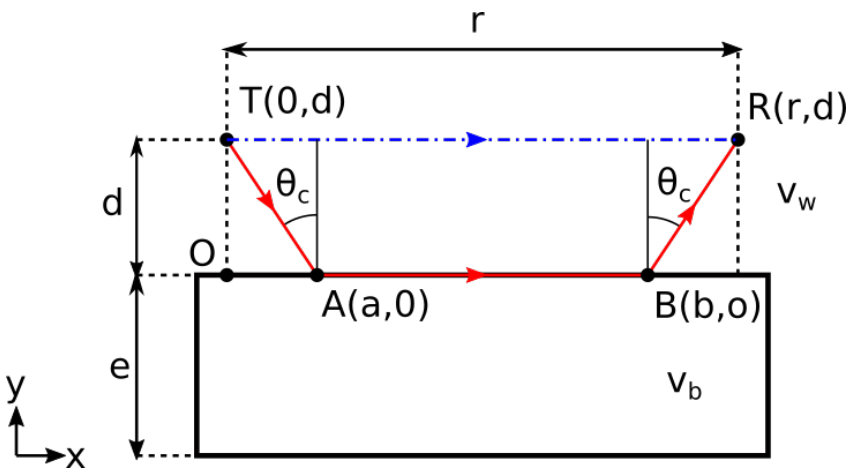

Figure 1: A drawing of the experimental setup. The rectangle with the solid borders is the bone sample. T is the transmitter and R is the receiver. O is the origin of the coordinate system, and A and B are the points where the head wave enters and exits the bone. The distance between the transmitter and the receiver is r, the vertical distance between the transmitter and the bone surface is d, and the thickness of the bone is e. θ_c is the critical angle that is described later in this report. The blue dot-dashed line corresponds to the path of the direct wave, while the solid red line corresponds to the head wave. The probe used in the actual measurements consists of 1 transmitter and 95 receivers in a fixed arrangement. This was modelled mathematically by varying the value of r.

In this section we will derive formula 2.3 for the critical angle. A similar derivation is done in Lowet et al., but here a different approach is used to motivate the generalisation of the method. The same setup as in the derivation of the flat bone trajectory is used. It is repeated above in figure 1.

When Lowet et al. first proposed the head wave axial transmission measurements for bones, they did not realise that they were using the head wave [2]. Instead, they only noted that the one of the signals was received much earlier than all other signals. They deduced that this signal must have propagated laterally through the bone, which has a much higher speed of sound than the surrounding material. By only making two assumptions they then derived the correct wave path, including the critical angle. The first of these assumptions was that the first arriving signal propagated at least some distance laterally through the bone. The second assumption was that waves take the shortest path in time (Fermat's principle). We make the same assumptions here.

The assumption that the wave travels at least some distance along the bone is the justification for the path shown in figure 1. In the experimental method, we derived the arrival time for a signal along this path:

$$t_{\text{head}} = \frac{\sqrt{a^2 + d^2}}{v_w} + \frac{b - a}{v_b} + \frac{\sqrt{(r - b)^2 + d^2}}{v_w} \tag{1}$$

It is now possible to find a and b, by our assumption that the head wave travels along the shortest path in time:

$$\frac{\partial t_{\text{head}}}{\partial a} = 0 \quad \text{and} \quad \frac{\partial t_{\text{head}}}{\partial b} = 0$$

Differentiating equation 1 with respect to a and b then gives:

$$\frac{a}{v_w\sqrt{d^2+a^2}} - \frac{1}{v_b} = 0 \quad \text{and} \quad \frac{1}{v_b} - \frac{(r-b)}{v_w\sqrt{(r-b)^2+d^2}} = 0 \tag{2}$$

Substitution of $1/v_b$ in the first equation using the second equation eventually gives $a = \pm(r-b)$. The assumption that the wave travels from left to right gives $a > 0$, $b > 0$, and $b > a$. Therefore only $a = r - b$ is valid. This agrees with the observation that the entry and exit angle of the head wave are equal, as seen in [2].

Directly solving the first condition in equation 2 gives:

$$a = \pm d\left(\sqrt{\left(\frac{v_b}{v_w}\right)^2 - 1}\right)^{-1} \tag{3}$$

Again assuming $a > 0$ means that only the positive solution is acceptable. Next, the arrival time of the head wave is calculated. Substituting $a = r - b$ into equation 1 gives:

$$t_{\text{head}} = \frac{2\sqrt{a^2+d^2}}{v_w} + \frac{r}{v_b} - \frac{2a}{v_b}$$

Finally substituting the value of a from equation 3 and simplifying gives:

$$t_{\text{head}} = \frac{r}{v_b} + \frac{2d}{v_w}\sqrt{1 - \left(\frac{v_w}{v_b}\right)^2} \tag{4}$$

Which agrees with equation 6 from [9], keeping in mind that in our model the transmitter and receiver have the same vertical position.

From the values of a and b, we can now calculate the critical angle. We have already seen that it is the same at the entry and exit point. By looking at figure 1 we can see that

$$\theta_c = \arctan\left(\frac{a}{d}\right)$$

If we then fill in a from equation 3, and note that (for $|x| < 1$)

$$\arctan(x) = \arcsin\left(\frac{x}{\sqrt{1+x^2}}\right)$$

we get

$$\theta_c = \arctan\left(\left(\sqrt{\left(\frac{v_b}{v_w}\right)^2 - 1}\right)^{-1}\right) = \arcsin\left(\sqrt{\frac{\left(\left(\frac{v_b}{v_w}\right)^2 - 1\right)^{-1}}{1 + \frac{1}{\left(\frac{v_b}{v_w}\right)^2 - 1}}}\right) = \arcsin\left(\frac{v_w}{v_b}\right) \Rightarrow \sin(\theta_c) = \frac{v_w}{v_b} \tag{5}$$

This is formula 2.3. This result agrees with the expressions given in [2] and [9].

Appendix B: Convergence test

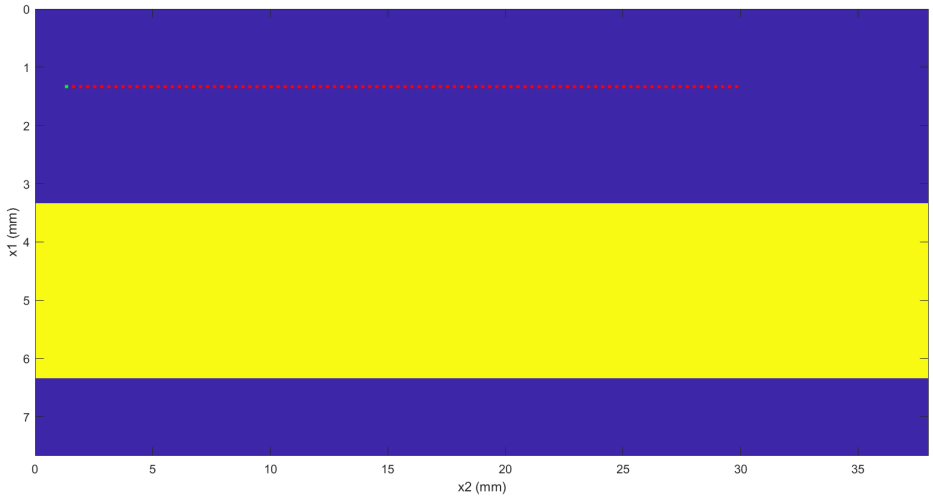

Figure 2: Plot of the simulation setup for the convergence test. The blue and yellow regions represent the soft tissue and the bone, respectively. The green dot is the location of an emitter, while the red dots are receivers

Methods

In order to validate the simulation, a convergence test was done. This test consists of four simulations on a simple geometry with a straight interface, as shown in figure 2. This geometry first consists of a margin of soft tissue between the receiver and simulation wall. This margin is exactly two times the wavelength of the signal in the bone. Below this, there is a layer of soft tissue that is 2 mm thick between the receivers and the surface of the bone. Then next layer is a 3 mm thick layer of bone, and finally there is another margin between the bone and the simulation edge. All layers are stacked vertically and are 38 mm wide. For each spatial step size $dx = 2.5, 5, 10, 15$ μm a simulation is made. The measurements were done by a P4-1 probe as described in table 2.2. The properties of the bone, and other simulation parameters, are shown in table 2.1. Both of these tables can be found in the experimental method section.

For each simulation, the semblance method is applied to calculate the speed of sound. This step is described in detail in the experimental method. Next, the signal received by receivers number 33, 50 and 83 is plotted for each simulation. These indices were chosen to correspond with 10,15 and 25 μm distance from the receiver, so the head wave should be visible at these points. By looking at these received signals, the convergence of the simulation to a correct solution can be observed as a function of dx.

Results

An x-t diagram from the convergence test for $dx = 5$ μm is shown in figure 3a. At first it was attempted to apply a Hilbert transform to this diagram, but this eventually caused the head wave and reflected wave to combine. By removing the Hilbert transform, however, the head wave can be distinguished along the entire trajectory. The x-t diagrams for $dx = 2.5$, 10 and 15 μm can be seen in figures 3b, 3c and 3d. At a first glance these diagrams appear very similar. However, the results obtained from these simulations are slightly different. For $dx = 5$ μm, the semblance method found a speed of 3.000 mm/μs, exactly the input of the simulation. However, for $dx = 10$ μm, the result was 3.004 mm/μs (0.14% error)

and for $dx = 15$ μm it was 3.006 mm/μs (0.2% error). Furthermore, the result for $dx = 2.5$ μm is 2.998 mm/μs (0.07% error). The semblance plots can be seen in figure 4. These plots show a smaller peak at a speed that is lower than the actual velocity. The amplitude of this peak decreases as dx becomes smaller, suggesting that it corresponds to a simulation error. Furthermore, the simulation becomes more accurate as dx becomes smaller, except for $dx = 2.5$ μm. We think that this exception may be the result of a smaller spatial step size requiring more calculations, and thus being more susceptible to small rounding errors.

Further analysis is done on the raw signals received at approximately 10, 15 and 25 μm from the transmitter, corresponding to receivers number 33, 50 and 83. The received signal for receiver number 33 is shown in figure 5. It can be seen that the signals appear to be similar, but that the amplitude quickly becomes higher for smaller spatial steps. This is probably caused by the fact that the receivers have a certain finite width. The simulation software accounts for this by summing the signal over all the gridpoints inside the receiver. A smaller spatial step means more gridpoints inside the receiver and thus a higher amplitude. To compensate for this effect, all the signals are normalised. The resulting signals can be seen in figure 6. Next, the part of all the signals that contains the head wave is analysed. Since all the receivers are far enough away from the transmitter, the headwave is the first signal to arrive at the receiver. The zoomed in plots are shown in figures 7a, 7b and 7c. It can be seen that different spatial step sizes still cause slight differences in amplitude between some peaks. However, $dx = 2.5$ and $dx = 5$ μm are very close together, much closer than the other signals.

Both $dx = 2.5$ and $dx = 5$ μm seem to provide correct results. However, $dx = 5$ μm is much quicker to simulate, so it was decided to use $dx = 5$ μm for all further measurements.

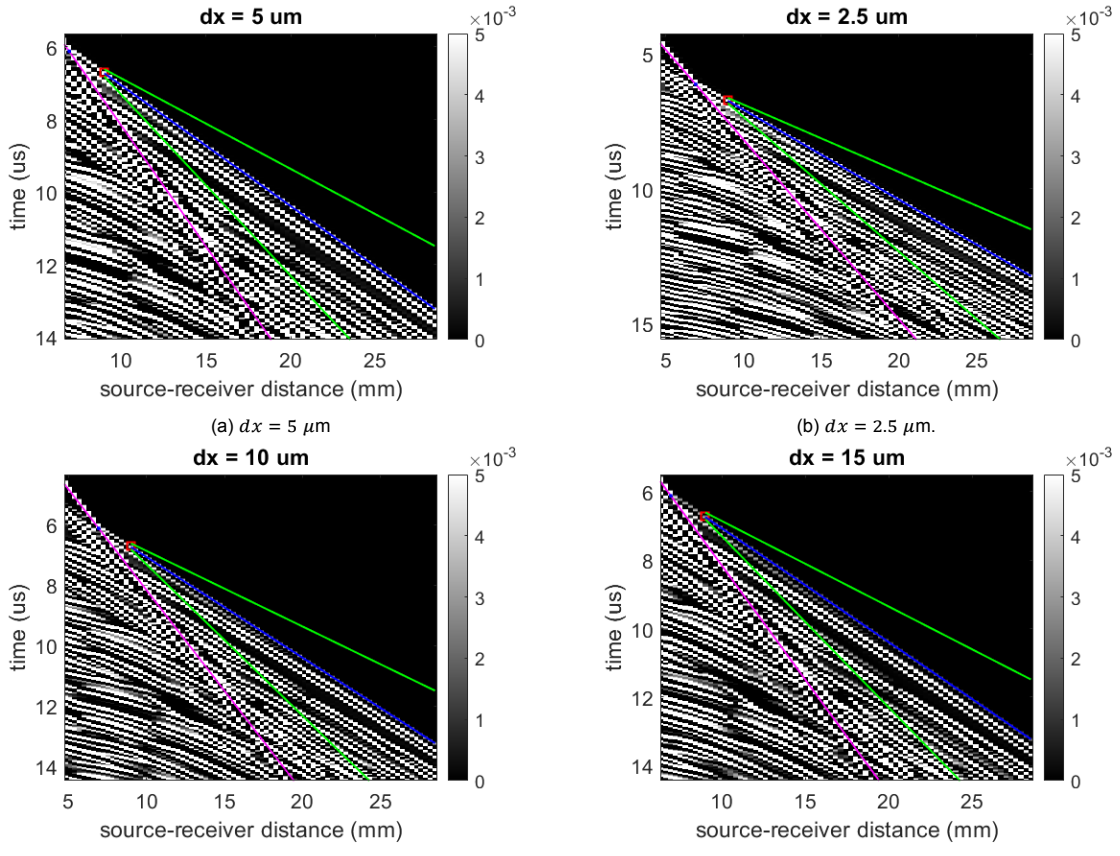

(a) $dx = 5$ μm

(b) $dx = 2.5$ μm.

(c) $dx = 10$ μm.

(d) $dx = 15$ μm.

Figure 3: x-t diagram for the 3 mm thick plate and various values for the spatial step dx. The speed of sound in the medium is 3 mm/μs, and excitation signal has a frequency of 4.5 MHz. The brightness at each point of the graph represents the vertical speed of the medium. The pink line corresponds to the direct wave, and the blue dot is the calculated point where the head wave intersects the direct wave. The green lines represent the outer limits of the mask, while the blue line corresponds to the trajectory found by the semblance method.

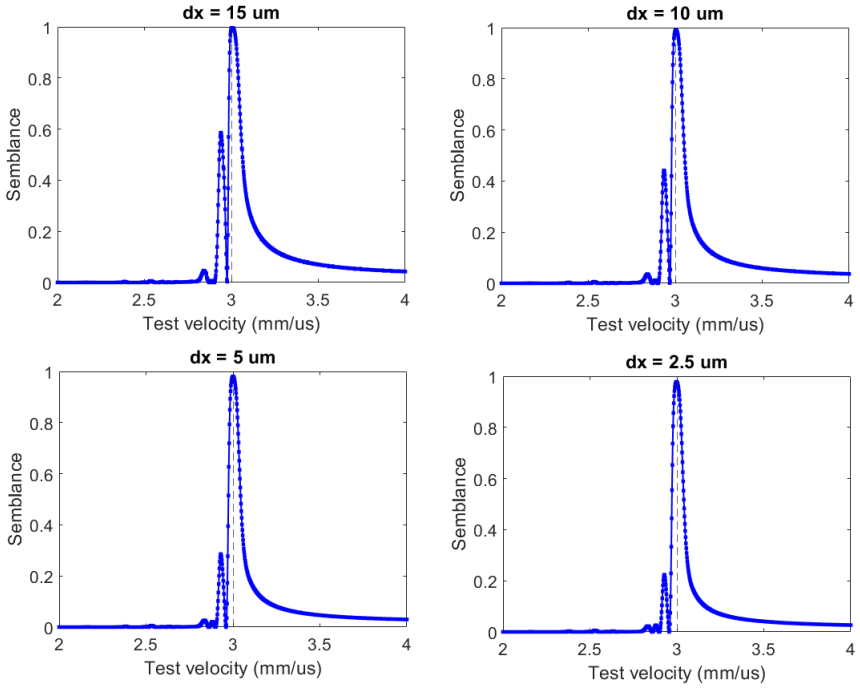

Figure 4: Semblance plot for four different values of the spatial step dx. The vertical axis is the semblance while the horizontal axis corresponds to the test velocity. For these plots the true velocity of the bone was 3 mm/μs

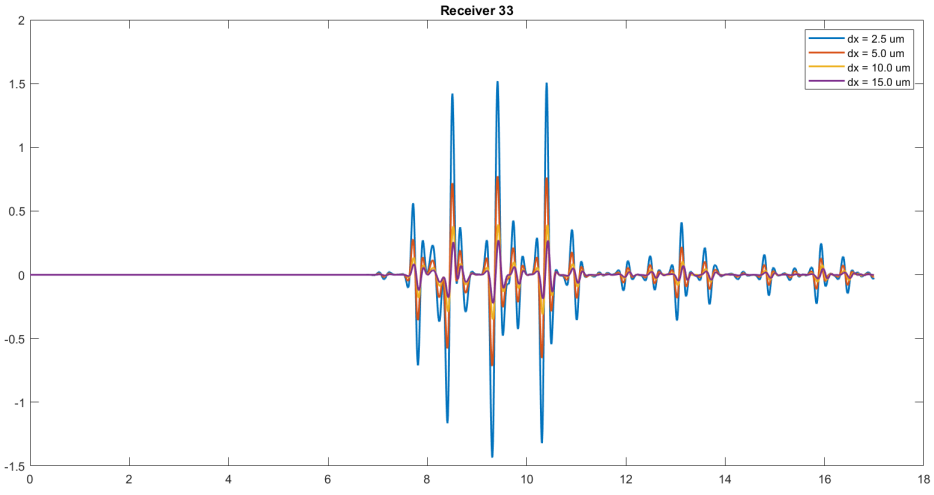

Figure 5: The signals at receiver number 33. Different line colours correspond to different spatial step sizes. The horizontal axis is the time in μs while the vertical axis is the intensity of the signal.

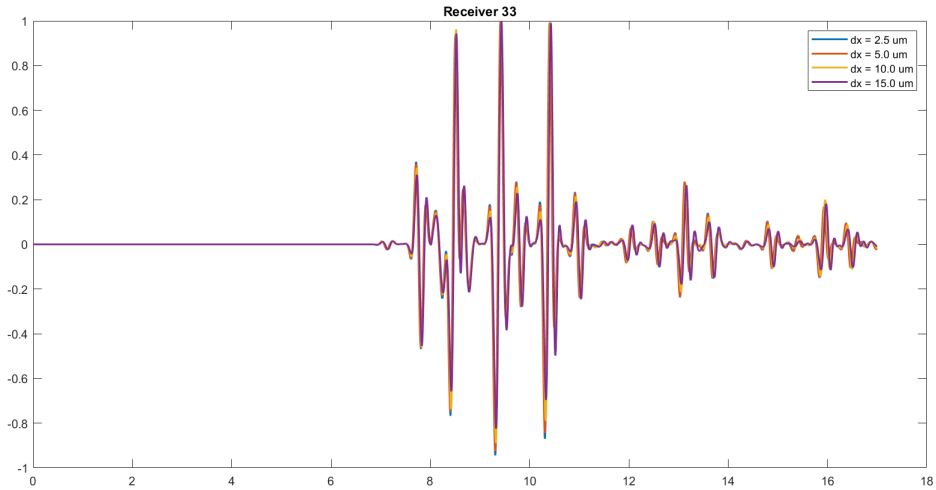

Figure 6: The signals at receiver number 33. All signals were normalised by dividing them by their maximum value. Different line colours correspond to different spatial step sizes. The horizontal axis is the time in μs while the vertical axis is the intensity of the signal.

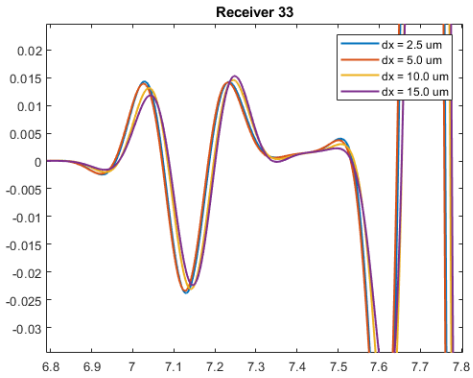

(a) Receiver number 33.

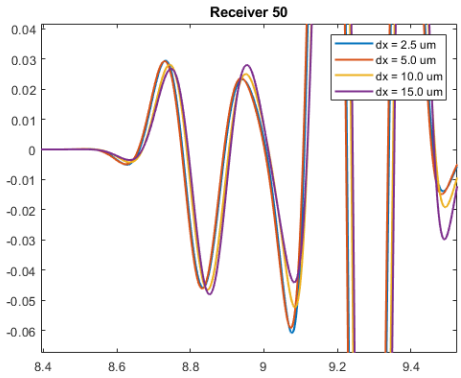

(b) Receiver number 50.

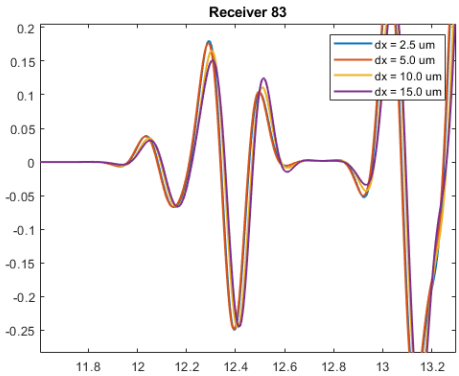

(c) Receiver number 83

Figure 7: The raw signals at three different receivers. The plot has been restricted to the part containing the head wave. All signals were normalised by dividing them by their maximum value. Different line colours correspond to different spatial step sizes. The horizontal axis is the time in μs while the vertical axis is the intensity of the signal.

Bibliography

[1] P. Moilanen, "Ultrasonic guided waves in bone," *IEEE Transactions on Ultrasonics, Ferroelectrics, and Frequency Control*, vol. 55, no. 6, pp. 1277–1286, 2008, ISSN: 08853010. DOI: 10.1109/TUFFC.2008.790.

[2] G. Lowet and G. Van der Perre, "Ultrasound velocity measurement in long bones: Measurement method and simulation of ultrasound wave propagation," *Journal of Biomechanics*, vol. 29, no. 10, pp. 1255–1262, 1996, ISSN: 00219290. DOI: 10.1016/0021-9290(96)00054-1.

[3] M. Mozaffarzadeh, C. Minonzio, N. De Jong, M. D. Verweij, S. Hemm, and V. Daeichin, "Lamb Waves and Adaptive Beamforming for Aberration Correction in Medical Ultrasound Imaging," *IEEE Transactions on Ultrasonics, Ferroelectrics, and Frequency Control*, vol. 68, no. 1, pp. 84–91, Jan. 2021, ISSN: 15258955. DOI: 10.1109/TUFFC.2020.3007345.

[4] M. Mozaffarzadeh, C. Minonzio, N. de Jong, M. D. Verweij, S. Hemm, G. Renaud, and V. Daeichin, "Erratum to "Lamb Waves and Adaptive Beamforming for Aberration Correction in Medical Ultrasound Imaging"," *IEEE Transactions on Ultrasonics, Ferroelectrics, and Frequency Control*, vol. 68, no. 2, pp. 352–353, Feb. 2021, ISSN: 0885-3010. DOI: 10.1109/TUFFC.2020.3045936. [Online]. Available: https://ieeexplore.ieee.org/document/9298803/.

[5] M. Mozaffarzadeh, E. Verschuur, M. D. Verweij, V. Daeichin, N. De Jong, and G. Renaud, "Refraction-Corrected Transcranial Ultrasound Imaging through the Human Temporal Window using a Single Probe," *IEEE Transactions on Ultrasonics, Ferroelectrics, and Frequency Control*, 2022, ISSN: 0885-3010. DOI: 10.1109/TUFFC.2022.3148121. [Online]. Available: https://ieeexplore.ieee.org/document/9698209/.

[6] M. Daugschies, K. Rohde, C. C. Glüer, and R. Barkmann, "The preliminary evaluation of a 1 MHz ultrasound probe for measuring the elastic anisotropy of human cortical bone," *Ultrasonics*, vol. 54, no. 1, pp. 4–10, 2014, ISSN: 0041624X. DOI: 10.1016/j.ultras.2013.07.004. [Online]. Available: http://dx.doi.org/10.1016/j.ultras.2013.07.004.

[7] M. Mozaffarzadeh, M. D. Verweij, V. Daeichin, N. De Jong, and G. Renaud, "Transcranial Ultrasound Imaging with Estimating the Geometry, Position and Wave-Speed of Temporal Bone," pp. 1–4, Nov. 2021, ISSN: 19485727. DOI: 10.1109/IUS52206.2021.9593826.

[8] E. Bossy, M. Talmant, and P. Laugier, "Three-dimensional simulations of ultrasonic axial transmission velocity measurement on cortical bone models," *The Journal of the Acoustical Society of America*, vol. 115, no. 5, pp. 2314–2324, 2004, ISSN: 0001-4966. DOI: 10.1121/1.1689960.

[9] E. Camus, M. Talmant, G. Berger, and P. Laugier, "Analysis of the axial transmission technique for the assessment of skeletal status," *The Journal of the Acoustical Society of America*, vol. 108, p. 3058, 2000. DOI: 10.1121/1.1290245. [Online]. Available: https://doi.org/10.1121/1.1290245.

[10] E. Bossy, M. Talmant, and P. Laugier, "Effect of bone cortical thickness on velocity measurements using ultrasonic axial transmission: A 2D simulation study," *The Journal of the Acoustical Society of America*, vol. 112, no. 1, pp. 297–307, 2002, ISSN: 0001-4966. DOI: 10.1121/1.1480836.

[11] E. Bossy, M. Talmant, M. Defontaine, F. Patat, and P. Laugier, "Bidirectional Axial Transmission Can Improve Accuracy and Precision of Ultrasonic Velocity Measurement in Cortical Bone: A Validation on Test Materials," *IEEE Transactions on Ultrasonics, Ferroelectrics, and Frequency Control*, vol. 51, no. 1, pp. 71–79, 2004, ISSN: 08853010. DOI: 10.1109/TUFFC.2004.1268469.

[12] G. Renaud, P. Kruizinga, D. Cassereau, and P. Laugier, “In vivo ultrasound imaging of the bone cortex,” *Physics in Medicine & Biology*, vol. 63, no. 12, p. 125 010, Jun. 2018, ISSN: 0031-9155. DOI: 10.1088/1361-6560/AAC784. [Online]. Available: https://iopscience.iop.org/article/10.1088/1361-6560/aac784%20https://iopscience.iop.org/article/10.1088/1361-6560/aac784/meta.

[13] I. Lerche, “On the reflection of acoustic waves from a slightly curved interface,” *The Journal of the Acoustical Society of America*, vol. 81, no. March, pp. 611–618, 1987.

[14] T. L. Pham, M. Talmant, and P. Laugier, “How does ultrasound bidirectional axial transmission reflect geometry of long bones?” *Proceedings - IEEE Ultrasonics Symposium*, pp. 229–232, 2008, ISSN: 10510117. DOI: 10.1109/ULTSYM.2008.0056.

[15] M. Gräsel, C. C. Glüer, and R. Barkmann, “Characterization of a new ultrasound device designed for measuring cortical porosity at the human tibia: A phantom study,” *Ultrasonics*, vol. 76, pp. 183–191, 2017, ISSN: 0041624X. DOI: 10.1016/j.ultras.2017.01.001.

[16] P. H. F. Nicholson, P. Moilanen, T. Kärkkäinen, J. Timonen, and S. Cheng, “Guided ultrasonic waves in long bones: Modelling, experiment and in vivo application,” *Physiological Measurement*, vol. 23, no. 4, pp. 755–768, 2002, ISSN: 09673334. DOI: 10.1088/0967-3334/23/4/313.

[17] M. Talmant, S. Kolta, C. Roux, D. Haguenauer, I. Vedel, B. Cassou, E. Bossy, and P. Laugier, “In vivo Performance Evaluation of Bi-Directional Ultrasonic Axial Transmission for Cortical Bone Assessment,” *Ultrasound in Medicine and Biology*, vol. 35, no. 6, pp. 912–919, 2009, ISSN: 03015629. DOI: 10.1016/j.ultrasmedbio.2008.12.008.